# Probing the pore of the auditory hair cell mechanotransducer channel in turtle

H. E. Farris, C. L. LeBlanc, J. Goswami and A. J. Ricci

*Neuroscience Center and Kresge Hearing Laboratories at Louisiana State University Health Sciences Center, New Orleans, LA 70112, USA*

**Hair cell mechano-electric transducer (MET) channels play a pivotal role in auditory and vestibular signal detection, yet few data exist regarding their molecular nature. Present work characterizes the MET channel pore, a region whose properties are thought to be intrinsically determined. Two approaches were used. First, the channel was probed with antagonists of candidate channel subtypes including: cyclic nucleotide-gated channels, transient receptor potential channels and gap-junctional channels. Eight new antagonists were identified. Most of the effective antagonists had a partially charged amine group predicted to penetrate the channel pore, antagonizing current flow, while the remainder of the molecule prevented further permeation of the compound through the pore. This blocking mechanism was tested using curare to demonstrate the open channel nature of the block and by identifying methylene blue as a permeant channel blocker. The second approach estimated dimensions of the channel pore with simple amine compounds. The narrowest diameter of the pore was calculated as 12.5 ± 0.8 Å and the location of a binding site ∼45% of the way through the membrane electric field was calculated. Channel length was estimated as ∼31Å and the width of the pore mouth at < 17 Å. Each effective antagonist had a minimal diameter, measured about the penetrating amine, of less than the pore diameter, with a direct correlation between $IC_{50}$ and minimal diameter. The $IC_{50}$ was also directly related to the length of the amine side chains, further validating the proposed pore blocking mechanism. Data provided by these two approaches support a hypothesis regarding channel permeation and block that incorporates molecular dimensions and ion interactions within the pore.**

(Resubmitted 15 January 2004; accepted after revision 2 June 2004; first published online 4 June 2004)
**Corresponding author** A. J. Ricci: Neuroscience Center and Kresge Hearing Laboratories, 2020 Gravier St Suite D, LSU Health Sciences Center, New Orleans LA 70112, USA. Email: aricci@lsuhsc.edu

Hair cells are the mechano-sensory cells of both auditory and vestibular systems, imparting sensitivity through mechano-electric transducer (MET) ion channels located at the tops of actin-filled stereocilia (hair bundle) (Fettiplace *et al.* 2001). Deflection of the hair bundle toward its tall edge opens MET channels while deflection away from the tall edge closes channels (Shotwell *et al.* 1981). Molecular identification of this channel has been elusive due to problems arising from the scarcity of expressed channels and the limited number of hair cells per sensory organ. Many MET channel properties including activation and adaptation kinetics, displacement sensitivity and perhaps even mechanical sensitivity may not be intrinsic to the channel but imposed by accessory proteins linking the channel to the cytoskeleton and\or to extracellular proteins, implying that when the putative channel is identified the expressed properties may differ significantly from native properties. However, channel pore characteristics should be intrinsic to the channel protein and should not vary due to accessory structures, thus providing a useful target for identification. The present work characterizes MET channel pore properties to gain insight into the molecular identity and to create a template upon which future molecular characterizations can be based.

The MET channel exhibits a non-specific cation conductance with a high calcium permeability (Ohmori, 1985; Crawford *et al.* 1991; Lumpkin & Hudspeth, 1995; Ricci & Fettiplace, 1998). MET channels pass large molecules such as tetraethyl ammonium and the membrane dye FM1-43 (Corey & Hudspeth, 1979; Gale *et al.* 2001). Single channel conductance estimates vary from 10 to 300 pS (Ohmori, 1985; Holton & Hudspeth, 1986; Crawford *et al.* 1991; Geleoc *et al.* 1997; Ricci *et al.* 2003). No voltage dependence of the channel (Ohmori, 1987; Crawford *et al.* 1991) has been reported. Biophysical

 DOI: 10.1113/jphysiol.2004.061267

characteristics suggest the channel is related to the broad class of non-specific cation channels that include the transient receptor potential channels (TRP), a subgroup of which are the vanniloid receptors (TRPV), cyclic nucleotide gated channels (CNG), mechanically gated channels, the nicotinic family of channels and even gap junctional hemi-channels. The presence of both CNG type and TRP type channels in hair cells (Kolesnikov *et al.* 1991; Liedtke *et al.* 2000; Drescher *et al.* 2002) make these channel classes prime candidates for the MET channel. With the identification of TRP-like channels regulating mechanosensation in *Drosophila* (Walker *et al.* 2000) and zebrafish (Sidi *et al.* 2003), a great deal of attention is being paid to the TRP family (Corey, 2003; Strassmaier & Gillespie, 2003). However, existing data cannot clearly classify the channel type.

Pharmacological data regarding MET channels are limited in that the blockers were not specific to channel classes, nor do they provide insight into the properties of the channel pore. For example, aminoglycoside antibiotics that can antagonize calcium channels, are open MET channel blockers (Ohmori, 1985; Kroese *et al.* 1989; Kimitsuki & Ohmori, 1993; Ricci, 2002). Amiloride and its derivatives, which block some CNG channels as well as channels of the epithelial sodium channel (ENAC) family (Frings *et al.* 1992; Kellenberger & Schild, 2002) also antagonize MET channels of hair cells as well as oocytes (Jorgensen & Ohmori, 1988; Lane *et al.* 1993; Rusch *et al.* 1994; Ricci, 2002). Tubocurarine, a nicotinic antagonist, also blocks the MET channel (Glowatzki *et al.* 1997). Cisplatin is yet another antagonist of the MET channel (Kimitsuki *et al.* 1993).

Present work creates a pharmacological profile of the MET channel pore to serve as a basis for comparisons with other known channel types and a template for the molecular identification and characterization of this channel. Eight new MET channel blockers were identified demonstrating the channel has broad similarities to other non-specific cation channels including the TRP and CNG channels. Furthermore, the molecular dimensions of the channel were estimated and support a novel open channel blocking hypothesis for charged amines.

## Methods

### Tissue preparation

Auditory papillae were prepared as previously described (Ricci & Fettiplace, 1997). Red-eared sliders (*Trachemys scripta elegans*), carapace length 8 to 15 cm were decapitated and the inner ear organs removed using procedures approved by the ACUC committee at LSU Health Sciences Center and conforming to standards established by NIH guidelines. The inner ear organs were placed into external solution containing (mM): 125 NaCl, 0.5 KCl, 2.8 $CaCl_2$, 2.2 $MgCl_2$, 2 each of pyruvate, creatine, lactate, ascorbate, 6 glucose and 10 Hepes. The solution was buffered to pH 7.6 and had a final osmolality of 275 mosmol $kg^{-1}$. The tissue was pinned to the bottom of a Sylgard-coated dish with minutien pins with the auditory papilla facing upward. The tectorial membrane was exposed and treated with protease type XXIV (Sigma) 0.02–0.04 mg $ml^{-1}$ for 5–20 min depending on enzyme activity. The tectorial membrane was removed with an etched tungsten wire and the enzyme removed with multiple rinses of external solution. The papilla was trimmed and placed into a coverslip-bottomed recording chamber and held in place with three single strands of dental floss. The recording chamber was perfused at a rate of 0.5–1 ml $min^{-1}$ with external solution supplemented with 100 nM apamin (Calbiochem) to block the caesium-permeable SK calcium-activated potassium current (Tucker & Fettiplace, 1996). A peristaltic pump (Gilson, Middleton, WI, USA) was used for the bath perfusion.

### Drug application

Drugs were applied to the apical surface through a 2 mm diameter pipette whose tip was pulled to an external diameter of ~75 $\mu$m. The pipette was placed about 100 $\mu$m away from the cell being recorded. Flow was perpendicular to the sensitive axis of the hair bundle (Ricci & Fettiplace, 1997). Flow rate was controlled using a Gilson peristaltic pump coupled through miniature solenoid valves (Lee Valves), the rate was maintained at 1–3 ml $h^{-1}$. Complete exchange of the apical fluid took 1.5 min. Measurements were made between 5 and 10 min after drug application. Toxins were pressure applied through a pipette of tip diameter 3–5 $\mu$m using a picospritzer (General Valve). Osmolality was varied by first lowering NaCl by 25 mM for the low osmolar solution and replacing with sucrose to raise osmolality to 275 (control) or 325 mosmol $kg^{-1}$ (high osmolar solution). This method allowed ionic strength to remain constant during changes in osmolality. Drugs were purchased from Fisher, Calbiochem and Sigma when necessary. Pseudecatoxin was a generous gift from Dr Moretti at Meiji Pharmaceutical University, Japan.

### Recording procedures

A large blunt pipette, filled with extracellular solution, was advanced into the papilla from the abneural edge while

applying pressure to the back end of the pipette, making a hole from which one to three cells could be removed to ensure good access. The location of the hole ($d$) is the relative position measured from the papilla apex. Unless otherwise stated, measurements were made from a high frequency location ($n = 136$, $d = 0.61 \pm 0.01$), while the average low frequency position was $0.39 \pm 0.05$ ($n = 50$). Whole cell recordings were obtained as has been previously described (Ricci & Fettiplace, 1997). An Axopatch 200 (Axon Instruments) was used for all recordings. The internal solution contained (mM): 110 CsCl, 3 MgATP, 5 creatine phosphate, 1 BAPTA, 10 Hepes, 2 ascorbate; pH was 7.2. Series resistances averaged $3.0 \pm 0.2$ MΩ ($n = 186$) after up to 70% compensation. Cell capacitance was $12.5 \pm 0.2$ pF ($n = 186$) giving voltage-clamp speeds of ∼38 μs. A junction potential of −4 mV was measured and corrected offline, as was any residual series resistance. Cells with leak currents greater than 50 pA, measured as non-mechanically gated inward current at −80 mV were excluded. Minimal leak subtraction was performed with the amplifier circuit. Cells were excluded if series resistance varied by more than 25% during the recording. All experiments were performed between 19 and 22°C.

Upon reaching whole cell configuration, calcium currents increased in amplitude for the first 10–15 min (Schnee & Ricci, 2003). Mechano-electric transducer (MET) currents also showed some limited run-up that was accompanied by a speeding up of adaptation and a slight leftward shift in the current–displacement plots. To account for these changes, data were not collected until the peak current had stabilized, about 10 min after break through.

### Mechanical stimulation

Hair bundles (see example in Fig. 1*A*) were stimulated with a stiff glass probe attached to a piezo-electric element (Ricci & Fettiplace, 1997). The voltage step to the piezo was filtered, with an 8-pole Bessel filter, at either 2 or 5 kHz to prevent exciting the intrinsic resonance of the ceramic. Probe motion was calibrated with a photodiode motion detector (Crawford & Fettiplace, 1985; Ricci *et al.* 2000). The glass probe, 1–1.5 μm in diameter, was placed near the bottom third of the bundle on the short stereocilia side so that the bundle was effectively pushed to open channels and pulled to close channels. Probe adherence to the bundle was enhanced by acid washing prior to use. On occasion, motion of the bundle was measured as a control to ensure probe adherence to the bundle (using the photodiode detector, Ricci *et al.* 2000). Activation protocols were driven by the Cambridge Electronic Device (CED) signal software. In some instances a piezo-electric stack was used (Jena), particularly for experiments where current–voltage relationships were investigated. The stack motion is axial compared to the ceramic, which is perpendicular to axial. The stimulus direction of the stack allowed for a larger diameter probe with better bundle contact that resulted in more reliable negative deflections which were essential for accurate measurements of MET currents at positive potentials.

### Data analysis

All data are presented as means ± S.E.M. The number of cells ($n$) is given with each set of data, usually for dose–response curves near the data point in the figure. Unless otherwise stated, current traces illustrated were averages of 16 sweeps for activation protocols and 4 sweeps for depolarization protocols. Data were collected with Signal software (CED) and exported to Origin (Microcal) or IGOR (Wavemetrics) for analysis. Origin uses the Levenberg-Marquardt algorithm for fitting. Where appropriate, correlation coefficients are given as $r^2$ values. Unless otherwise stated, Student's two-tailed $t$ tests were used to assess statistical significance ($P < 0.01$).

Maximal currents were obtained by adding the current amplitudes measured from saturating positive and negative hair bundle displacements (Fig. 1*B*). Responses were determined to be saturating by fitting the peak current plotted against stimulus amplitude with the equation for a double Boltzmann function (see Fig. 1*B*; Ricci & Fettiplace, 1997):

$$I/I_{\max} = 1/\{1 + (\exp(a_1 x_1 - a_1 x)) \times (1 + \exp(a_2 x_1 - a_2 x))\} \quad (1)$$

where $a_1$ and $a_2$ determine the steepness and $x_1$ determines the position along the displacement axis for both processes (for simplicity, $x_1 = x_2$). Generating a full activation curve ensured saturating stimuli. The current–voltage plots used only a single large positive and negative step, the amplitude predetermined from an activation curve generated at a holding potential of −80 mV.

Current ratios, $I_{\text{ion}}/I_{\text{Na}}$, rather than reversal potential shifts were used for both comparison of monovalent permeabilities and amine permeabilities. This method is necessary because removing calcium irreversibly abolishes transduction (Assad *et al.* 1991; Crawford *et al.* 1991) and lowering calcium can alter the single channel conductance (Ricci *et al.* 2003). It was necessary to maintain calcium at a constant level while altering the species of monovalent ion. It is assumed that part of the current carried

under each condition was calcium, a hypothesis supported by the maintenance of some adaptation in the presence of amines or antagonists. Current ratios can be used as estimates of permeability as long as the independence principal is satisfied (Hille, 1973). Monovalent ions have not been shown to interact in the pore, thereby meeting the criteria, though divalents have. The interaction between divalents and monovalents is assumed a constant for these experiments. Further experimental justification of this methodology is presented in the results.

Dose–response curves were fitted with a Hill equation:

$$I_{\text{blocked}}/I_{\max} = B_{\max}(x^n/(k^n + x^n)) \quad (2)$$

where $k$ is the half-blocking dose ($IC_{50}$) and $n$ is the Hill coefficient. $B_{\max}$ is the maximal block obtained. Throughout the paper dose–response curves are plotted as $I_{\text{drug}}/I_{\text{control}}$, which results in the Hill coefficient being negative; the absolute values are presented for simplicity. All dose–response curves are plotted using the maximal current elicited before additional open channel block was obtained. For curare both peak and steady-state values are presented.

### Molecular dimensions

The dimensions of the amine compounds and drugs were determined by building Corey-Pauling-Koltun (CPK) space filling models (Adams *et al.* 1980). The orientation of the models was first determined using energy minimalization in Chem3D software (Cambridge, Cambridge, MA, USA). For the amine derivatives, the diameter was measured as the diameter of the smallest circle that the molecule could pass through. Three measurements were made from the antagonists, the minimal diameter of the region of the molecule proposed to penetrate the channel pore, the maximal width proposed to prevent permeation of the compound and the distance between these two measurements. The first two measurements were made in an identical manner to that of the simple amine compounds, the latter was measured with a calliper calibrated for the size of the model molecules.

### Pore diameter

In Fig. 10*C* two theoretical fits are given to the plot of ionic radius against relative permeability. The first assumes a circular pore and spherical amines. The relationship between relative permeability and ionic radius is then equivalent to:

$$I_x/I_{\text{Na}} = A(1 - a/r)^2 \quad (3)$$

where $I_x/I_{\text{Na}}$ is the current ratio, $a$ is the radius of the amine compound, $r$ is the radius of the pore and $A$ is a scaling factor. The second model included a term for viscous drag as a function of the size of the amine ($a$). The relationship is given as:

$$I_x/I_{\text{Na}} = (A(1 - a/r)^2)/a \quad (4)$$

where all terms are as described above. This analysis is much the same as that used for investigating endplate currents (Adams *et al.* 1980) and sodium channels (Sun *et al.* 1997) and allows for an estimate of the dimensions of the smallest region of the MET channel pore.

### Location through membrane electric field

A single site blocking model was fitted to current–voltage data obtained in the presence of different antagonists and *n*-alkyl-amine compounds of the form:

$$I/I_{\max} = k[\exp((1 - \delta)(V - V_r)/V_s) - \exp(-\delta(V - V_r)/V_s)] \quad (5)$$

where $k$ is a proportionality constant, $\delta$ is the fractional distance through the membrane electric field traversed by the amine, $V_r$ is the reversal potential and $V_s$ reflects the steepness of rectification (Woodhull, 1973; Kros *et al.* 1992; Rusch *et al.* 1994; Gale *et al.* 2001). Although the MET channel is a multi-ion pore where interactions between ions have been suggested (Lumpkin *et al.* 1997; Ricci & Fettiplace, 1998), this simple single energy barrier model adequately fits the data presented.

### Pore length

Knowing the single channel conductance and the diameter of the pore allows for the estimate of the length of the channel. This estimate assumes a cylindrical shape to the pore. Rearrangement of the original equations (Hille, 1968) gives:

$$L = \rho g((\pi D/\rho g)^2 - 2/\pi^2)/4\pi \quad (6)$$

where $\rho$ is the resistivity of the solution (100 Ω cm), $g$ is the single channel conductance, $D$ is the diameter of the pore, $L$ is the length of the channel.

## Results

MET currents were obtained from hair cell recordings in the isolated turtle auditory papilla, where the apical hair bundle protruded upward from the apical surface (Fig. 1*A*). Hair bundles were stimulated with square displacement steps of increasing amplitude (Fig. 1*B*).

Peak current amplitude was plotted against stimulus amplitude to generate activation curves (Fig. 1*C*) which were analysed by fitting the data with a double Boltzmann eqn (1). Activation curves fitted with Boltzmann functions gave the most reliable measure of the peak current elicited and so were used in the presence of drugs to ensure accurate estimates of drug effects. Saturating steps also resulted in adaptation being slowed so as not to

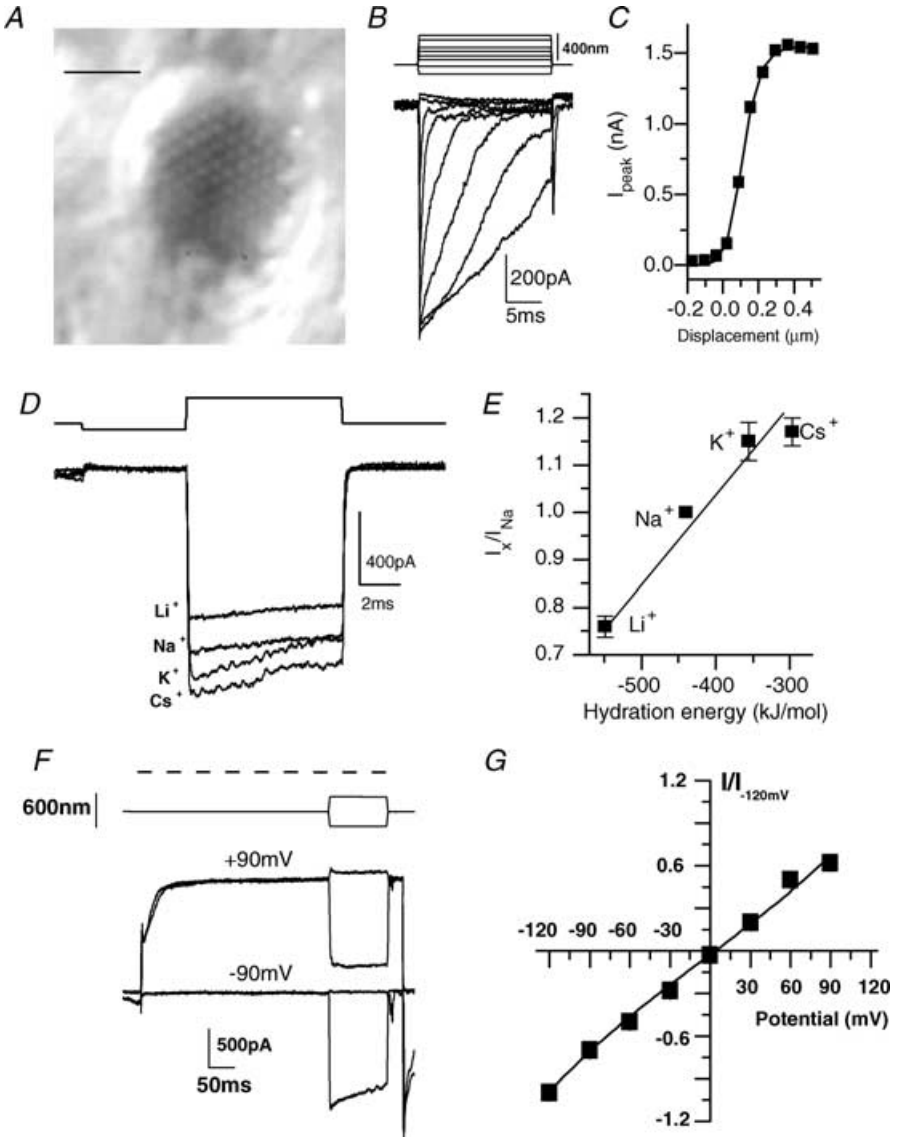


**Figure 1. Mechano-electric transducer (MET) channels are non-specific and non-rectifying**
*A*, Nomarski image of the apical surface of a hair cell revealing the array of actin-filled stereocilia; scale bar 5 $\mu$m. *B*, response of a hair cell, voltage-clamped at −80 mV, to a series of increasing amplitude mechanical deflections of the hair bundle (stimulus shown above, where upward indicates toward the kinocilium). *C*, plotting the peak current against hair bundle deflection (squares) gives a sigmoidal shaped response best fitted by a double Boltzmann equation (eqn (1); indicated by curve), with values of $a_1 = 16 \pm 7\ \mu m^{-1}$, $a_2 = 20 \pm 10\ \mu m^{-1}$ and $x_1 = 0.06 \pm 0.003\ \mu m$ ($r^2 = 0.99$; $x_1 = x_2$). *D*, saturating currents were elicited in the presence of different monovalent ions to investigate the current-passing ability of these cations. *E*, current ratios were directly correlated to the hydration energy of the ion. A linear regression with a slope of 0.0017 mol $kJ^{-1}$ and a *Y*-intercept of 1.71 were obtained ($r^2 = 0.98$). *F*, maximal MET currents were recorded at different membrane potentials. Dashed line refers to duration of voltage step. Mechanical stimuli are shown above current records. Currents evoked at ± 90 mV are given as examples (see text for description). Plots of MET current normalized to the current at −120 mV against membrane potential are given in *G* for 7 cells. The fit is to eqn (5), where $K = 0.59 \pm 0.07$, $\delta = 0.45 \pm 0.01$, $V_r = 7 \pm 1$ mV and $V_s = 52 \pm 5$ mV ($r^2 = 0.99$).

interfere with determining the open channel nature of some of the blockers (Fig. 1*B*). It should be noted that significant adaptation can still occur when the peak MET current has been obtained (Fig. 1*B*; peak current amplitude is saturated in last three responses).

Ion substitution experiments were performed by replacing $Na^+$ ions with the test monovalent ion in the apical perfusion solution (Fig. 1*D*). Replacement with $K^+$, $Cs^+$ and $Li^+$ demonstrated that the channel followed a permeation order directly correlated with the ion's hydration energy (Fig. 1*E*) (Edsall & McKenzie, 1978). The order $Cs^+ > K^+ > Na^+ > Li^+$ followed an Eisenmann series XI, in good agreement with previous investigations using reversal potential measurements (Ohmori, 1985) and indicative of a channel with a negatively charged external mouth (Adams *et al.* 1980). The agreement with reversal potential estimates supports the accuracy of using current ratios in these investigations. The minimally rectifying, non-specific conductance of the channel was also verified by measuring peak currents at various membrane potentials (Fig. 1*F* and *G*). Depolarizations reduce the driving force for calcium entry, resulting in a leftward shift of the MET activation curve (Eatock *et al.* 1987; Crawford *et al.* 1989). The example in Fig. 1*F* illustrates this phenomenon at +90 mV. Here, outward MET current turns on during depolarization as the activation plot shifts leftward due to the decrease in intraciliary $Ca^{2+}$. Mechanical deflection of the hair bundle away from the kinocilium turns the MET current off, seen as a reduction in outward current. Comparison of the relative current turned off and on mechanically at $\pm$ 90 mV illustrates the large leftward shift in activation. Current amplitudes for the current–voltage plots (Fig. 1*G*) were measured as the net current evoked from positive and negative hair bundle deflections (Fig. 1*F*). The reversal potential was $7 \pm 1$ mV ($n = 7$; eqn 5) suggesting a non-specific cation channel. The comparable currents obtained at positive and negative potentials demonstrate the minimally rectifying nature of the current. These results are in good agreement with previous investigations (Ohmori, 1985; Crawford *et al.* 1989). In the presence of a drug, eqn (5) estimates the distance through the electric field the drug travels until bound ($\delta$). In control, however, $Ca^{2+}$ is the blocking agent and eqn (5) gives an estimate of the distance $Ca^{2+}$ travels to its blocking site (Kros *et al.* 1992; Gale *et al.* 2001). An estimate of $0.45 \pm 0.01$ was obtained, suggesting the binding site is near the middle of the electric field and in reasonable agreement with previous work in chick (Kimitsuki & Ohmori, 1993), bullfrog (Kroese *et al.* 1989) and mouse (Kros *et al.* 1992; Gale *et al.* 2001). This estimate supports previous arguments that the blocking site for $Ca^{2+}$ and the binding site for fast adaptation may be different (Crawford *et al.* 1991; Ricci *et al.* 1998).

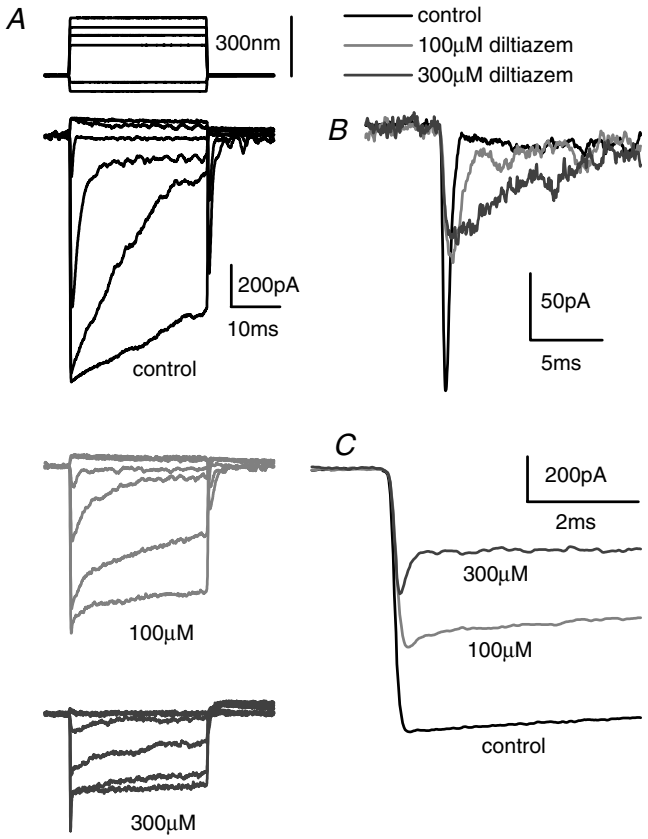


**Figure 2. Diltiazam blocks the MET current, slowing adaptation and showing some evidence for open channel block**
*A*, stimulus shown at top, with upward indicating towards kinocilium, MET currents for control (black, upper panel), 100 $\mu$M diltiazem (grey, middle traces) and 300 $\mu$M diltiazem (lower, dark grey traces) are shown. Scale bar near control traces should be used for all drug doses. *B*, expanded view of the smallest response to hair bundle deflection, demonstrating that fast adaptation slows as the MET current was reduced. *C*, expanded view of largest stimulus demonstrating that in the presence of the drug, the current shows a rapid decrease in amplitude, indicative of an open channel block.

### Cyclic nucleotide-gated (CNG) channel antagonists

CNG channel antagonists were investigated first using the benzothiazepine derivative diltiazem and the acetonitrile derivative D600, normally considered L-type calcium channel blockers, but also potent antagonists of CNG channels (Frings *et al.* 1992; Kleene, 2000). Diltiazem's effect on MET currents is presented in Fig. 2*A*, where responses to different amplitude stimuli are shown in the absence and presence of two doses of the drug. Both fast and slow adaptation were slowed by the antagonist.

The effect on fast adaptation is more clearly illustrated in Fig. 2*B*, an expanded view of the response to the smallest bundle stimulus (Fig. 2*A*). As the diltiazem concentration was increased, adaptation was slowed. Effects on adaptation were best observed from responses to small mechanical hair bundle deflections. With larger deflections, used to obtain maximal currents, a fast decay in current was observed in the presence of diltiazem that was not observed in the absence of the drug (Fig. 2*A* and *C*). This type of response is often, though not always, observed with open channel blockers (Armstrong, 1971; French & Shoukimas, 1981). It was previously argued that the ability

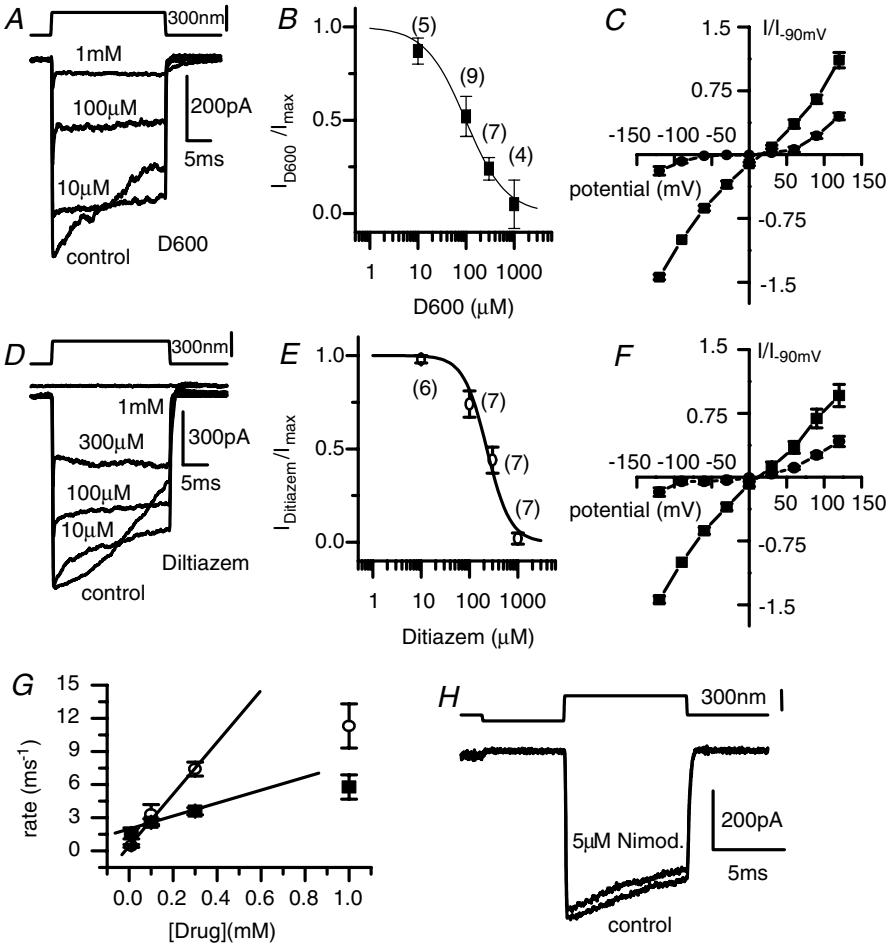


**Figure 3. Both diltiazem and D600, known cyclic nucleotide-gated channel blockers are effective antagonists of the MET channel**

Examples of the effects are given in *A* and *D* where saturating MET currents were elicited in various concentrations of drug at a holding potential of −80 mV. The dose–response curves with corresponding fits to the Hill equation are given in *B* and *E* for each drug. D600 had an $IC_{50}$ of $110 \pm 10$ $\mu$M and a Hill coefficient of $1.0 \pm 0.1$ ($r^2 = 0.99$). Diltiazem had an $IC_{50}$ of $228 \pm 22$ $\mu$M and a Hill coefficient of $1.8 \pm 0.3$ ($r^2 = 0.98$). The number of cells is given in parenthesis next to the data point. The voltage dependence of block for both D600 (*C*) and diltiazem (*F*) was assessed using the protocol defined in Fig. 1*F* ($n = 5$ for each; ■, in the absence of blocker; ●, in the presence of blocker). The fits to eqn (5) for control data are shown as continuous lines where $K = 0.29 \pm 0.02$ and $0.29 \pm 0.02$, $\delta = 0.47 \pm 0.01$ and $0.47 \pm 0.01$, $V_r = 13 \pm 1$ mV and $14 \pm 2$ mV and $V_s = 42 \pm 2$ mV and $42 \pm 2$ mV ($r^2 = 0.99$) for D600 and diltiazem, respectively. *G*, the decay in current attributed to the drug could be fitted by an exponential, from which the rate (1/time constant) was plotted against dose for each drug. A linear fit, indicative of a first order reaction, which has a slope equivalent to the rate constant, is given using only the first three values. As the rate for the highest concentrations was limited by voltage-clamp speed it was not included in the fit. The slope was $2.4 \pm 0.2$ ms$^{-1}$ mM$^{-1}$ ($r^2 = 0.99$) for diltiazem and $1.8 \pm 0.2$ ms$^{-1}$ mM$^{-1}$ ($r^2 = 0.98$) for D600. *H*, nimodipine, another L-type calcium channel blocker, not known to block cyclic nucleotide-gated channels was ineffective in blocking the MET current at 5 $\mu$M. The protocol used here allowed for maximal positive and negative stimulation.

to detect the drug-induced decay in current was in part determined by the kinetics of the channel (Ricci, 2002). Larger deflections of the hair bundle result in the channel open time increasing, thus promoting the observation of the open channel block (Ricci *et al.* 2003) and supporting the hypothesis regarding kinetics.

Both diltiazem and D600 were effective at antagonizing the MET channel (Fig. 3*A* and *D*). Maximal current responses in the presence of varying concentrations of drugs are illustrated in Fig. 3*A* and *D*. The dose–response curves for each compound are plotted in Fig. 3*B* and *E*, with fits to the Hill eqn (2) given as continuous lines. Diltiazem had an $IC_{50}$ of $228 \pm 22$ $\mu$M and a Hill coefficient of $1.8 \pm 0.3$ ($r^2 = 0.98$). D600 had an $IC_{50}$ of $110 \pm 10$ $\mu$M and a Hill coefficient of $1.0 \pm 0.1$ ($r^2 = 0.99$). Although, the $IC_{50}$ for D600 is comparable to that of olfactory CNG channels, the $IC_{50}$ for diltiazem is several-fold lower than the value obtained for CNG channels (Frings *et al.* 1992).

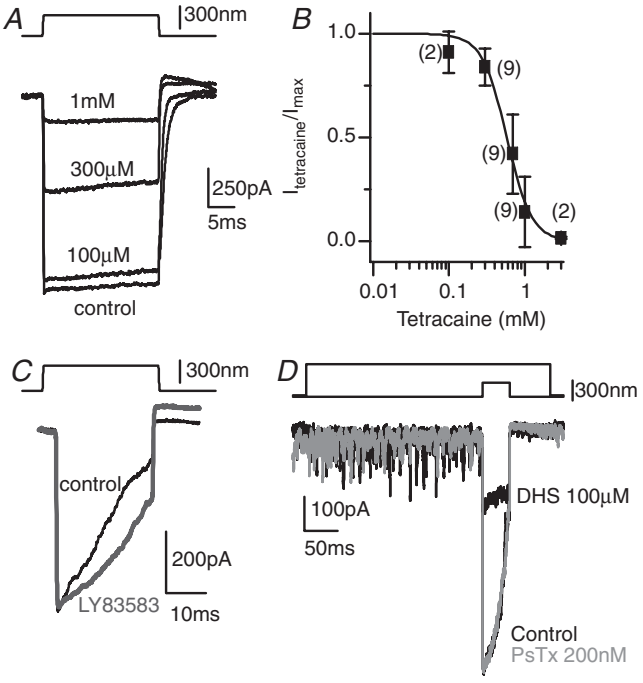


**Figure 4. Other classes of CNG blockers have variable effects on MET currents**

*A*, examples of saturating currents in the absence and presence of different concentrations of tetracaine, a local anaesthetic. *B*, the dose–response curve for tetracaine was fitted with the Hill equation, giving an $IC_{50}$ of $579 \pm 39$ $\mu$m, and a Hill coefficient of $2.7 \pm 0.4$ ($r^2 = 0.98$). *C*, a third type of cyclic nucleotide-gated channel blocker, LY83583, was ineffective at antagonizing the MET current. *D*, pseudecatoxin (PsTx), another known antagonist of CNG channels, was applied to the apical surface with a picospritzer to conserve volume and limit artifacts due to toxin sticking to tubing (single traces shown). As a control, dihydrostreptomycin was applied first, to adjust positioning and ensure a proper flow of drug. A separate pipette was used for each drug. PsTx had no effect on the peak transducer current at concentrations up to 200 nM.

A small rapid decay in current was observed in the presence of each drug, indicative of an open channel block (Armstrong, 1971; French & Shoukimas, 1981). Time constants were obtained from the decay in current by fitting the data with a simple exponential equation. The rate ($1/\tau$, obtained from the exponential fit) was plotted against dose for each compound in Fig. 3*G* and best fitted with a linear regression indicative of a first order reaction where the slope of the line represents the rate constant. Slope values of $1.8 \pm 0.2$ and $2.4 \pm 0.2$ ms$^{-1}$ mM$^{-1}$ were obtained for D600 and diltiazem, respectively. The fastest values for each compound were not included in the fit as they were limited by the voltage-clamp speed of the recording. A first order reaction is consistent with an open channel block. The block by D600 and diltiazem was voltage-dependent, with little of the MET current being blocked at +80 mV (data not shown).

The voltage dependence of block was also investigated for both diltiazem and D600 (Fig. 3*C* and *F*, $n = 5$). In both cases block was removed as the cell was depolarized, supporting the argument of an open channel blocker. Slight removal of block was also observed at hyperpolarized potentials. Although this might be interpreted as representing a permeable block by these compounds, it is unlikely (see Discussion). For D600, complete block of the current was not obtained at 1 mM and so the increased current may simply reflect the increased driving force for this unblocked portion. Higher doses were attempted but solubility became an issue and so those data are not included. For diltiazem, the release is postulated to reflect calcium or monovalent ions being forced passed the compound in the pore of the channel (see Discussion for explanation).

Both D600 and diltiazem are L-type calcium channel blockers that bind to overlapping regions of the channel's $\alpha$-subunit (Kraus *et al.* 1996), a similar location to the dihydropyridine binding site. Because dihydropyridines block L-type calcium channels but not CNG-gated channels (though see Zufall & Firestein, 1993), nimodipine was applied to the apical surface at 5 $\mu$M. No significant effect was observed on the MET current ($n = 3$), suggesting the ability of diltiazem and D600 to antagonize the MET current was not a function of a similarity between the MET channel and L-type calcium channels (Fig. 3*H*).

Local anaesthetics such as tetracaine also block CNG channels, a block postulated to occur by binding to the channel's closed state (Fodor *et al.* 1997). Tetracaine potently antagonized the MET current (Fig. 4*A*). Figure 4*B* shows the dose–response relationship and Hill equation

fit with values for $IC_{50}$ of $579 \pm 39$ $\mu$M and Hill coefficient of $2.7 \pm 0.4$, values consistent with the block of a CNG channel. No decay in current during the stimulus was observed.

Together the block of the MET current by tetracaine, diltiazem and D600 are consistent with the MET channel pore being similar to that of CNG-gated channels. To further test this hypothesis the novel CNG antagonist LY83583, a guanylyl cyclase inhibitor, was applied at concentrations up to 10 $\mu$M (Leinders-Zufall & Zufall, 1995), but was ineffective at blocking the MET current (Fig. 4*C*). In addition, pseudecatoxin (PsTx), a toxin isolated from the Australian King Brown snake that antagonizes a variety of CNG channel types (Brown *et al.* 1999), was applied via picospritzer to the apical hair bundle just prior to and during a mechanical stimulation (Fig. 4*D*). The picospritzer was used due to the small quantity of toxin available. No effect of PsTx was observed on the MET channel (200 nM, $n = 5$). Dihydrostreptomycin served as the control drug to demonstrate that picospritzer application of the compound could effectively antagonize the MET current. The increased baseline noise was evidence that the flow from the picospritzer was stimulating the hair bundle. Thus, although our results suggest the MET channel has some similarities with CNG channels, they do not provide unequivocal evidence that the channel is a member of the CNG family, as only some of the antagonists were effective.

### Transient receptor potential (TRP) channels

TRP channels represent a broad and growing class of non-specific cation channels (Clapham *et al.* 2001; Benham *et al.* 2002; Montell *et al.* 2002). Due to their diversity and novelty, the pharmacology of these channels has not been well characterized. However, there are several known antagonists. Trivalent ions such as lanthanum antagonize TRP channels (Halaszovich *et al.* 2000). $La^{3+}$ antagonized the MET current quite potently, with an $IC_{50}$ value of $3.8 \pm 0.7$ $\mu$M and a Hill coefficient of $0.7 \pm 0.1$ (Fig. 5*A* and *B*). Gadolinium, another trivalent compound, also blocked the MET current (Kimitsuki *et al.* 1996). Both of these trivalent molecules are not TRP selective and block other mechanically gated channels, including those of baroreceptors (Kraske *et al.* 1998), TRAAK channels (Maingret *et al.* 1999) and oocyte mechano-gated channels (Wilkinson *et al.* 1998). The overlap in blocking ability may represent similarities in the pores of mechanically gated channels.

A second TRP channel antagonist, ruthenium red, antagonized the MET current (Gunthorpe *et al.* 2002) (Fig. 5*C* and *D*). The $IC_{50}$ for block was $3.6 \pm 0.9$ $\mu$M and the Hill coefficient was $1.4 \pm 0.1$. The sensitivity to both trivalents and ruthenium red provides stronger evidence for a similarity with TRP channels. In the example shown, a large reduction in adaptation is apparent, despite, at the lowest doses, a relatively small effect on current amplitude.

The vanilloid receptor channels constitute a subclass of the TRP family (Gunthorpe *et al.* 2002). Recent evidence demonstrates the presence of an osmotically activated vanilloid receptor in hair cells (Liedtke *et al.* 2000). The effects of osmolality, pH and capsaicin on MET currents were investigated ($n = 3$ for each). Changes of $\pm 50$ mosmol $kg^{-1}$ using sucrose substitution did not alter the MET response. pH variations of $\pm 1$ unit also did not alter the MET current, and capsaicin application (200 nM) had no effect on the MET current (see Table 1). These data

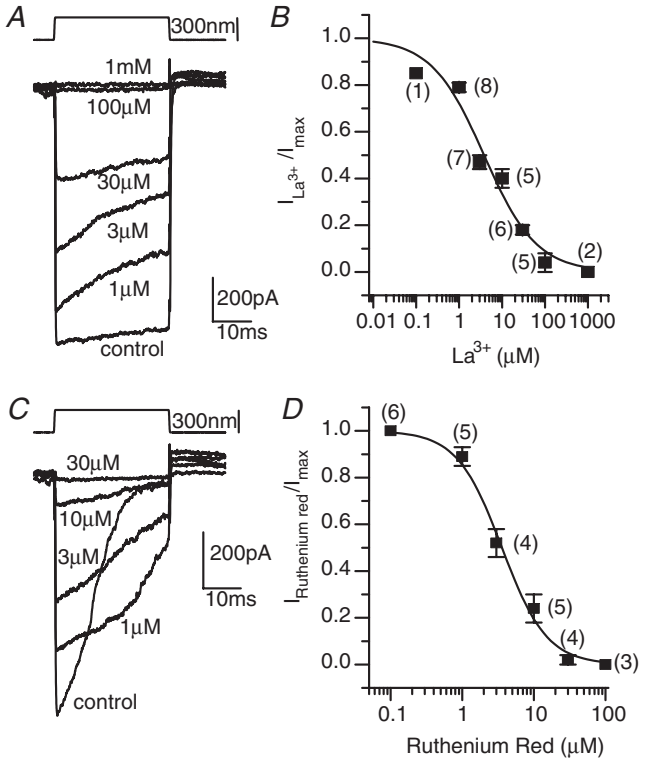


**Figure 5. TRP channel antagonists ruthenium red and lanthanum both blocked the MET current in a dose-dependent manner**

*A*, saturating currents were mechanically elicited in the absence and presence of various concentrations of lanthanum; stimulus shown above. *B*, the dose–response curve was plotted from maximal currents (■) and best fitted by a Hill equation with a coefficient of $1.4 \pm 0.2$ and an $IC_{50}$ of $3.6 \pm 0.3$ $\mu$M ($r^2 = 0.99$). *C*, saturating MET currents were elicited in the absence and presence of ruthenium red. *D*, dose–response curve was generated from maximal currents (■) and best fitted with a Hill equation with a coefficient of $0.7 \pm 0.1$ and an $IC_{50}$ of $3.8 \pm 0.7$ $\mu$M ($r^2 = 0.99$).

**Table 1. Summary of pharmacological sensitivities of the hair cell MET channels**

| Drug | Action | Minimum diameter (Å) | Maximum diameter (Å) | Length (Å) | *n* | Concn | % block | $IC_{50}$ | Hill coefficient |
|---|---|---|---|---|---|---|---|---|---|
| 4AP | K-type | **5.1** | 5.1 | 4.34 | 4 | 1 mM | $5 \pm 6$ | — | — |
| TEA | K-type | **9.0** | 9 | 7.9 | 5 | 1 mM | NE | — | — |
| Diltiazem | Ca/CNG | **6.5** | **14.3** | 16.95 | | DRC | 100 | $228 \pm 22$ μM | $1.8 \pm 0.3$ |
| D600 | Ca/CNG | **6.5** | **14.8** | 21.6 | | DRC | 100 | $110 \pm 10$ μM | $1 \pm 0.1$ |
| Nimodipine | Ca | 11.4 | **18.1** | 16.2 | 3 | 5 μM | NE | — | — |
| Tetracaine | CNG/Na | **6.9** | 9.1 | 16.5 | | DRC | 100 | $579 \pm 39$ μM | $2.7 \pm 0.4$ |
| Pseudecatoxin | CNG | — | — | — | 4 | 200 nM | NE | — | — |
| LY83583 | CNG | **8.7** | 8.7 | 13 | 4 | 100 μM | NE | — | — |
| Ruthenium Red | TRP | **9.7** | 9.7 | 13.2 | | DRC | 100 | $3.6 \pm 0.3$ μM | $1.4 \pm 0.2$ |
| Lanthanum | TRP | — | — | — | | DRC | 100 | $3.8 \pm 0.7$ μM | $0.7 \pm 0.1$ |
| Curare (pk) | ACH | **9** | **17.4** | 17.5 | | DRC | 100 | $16 \pm 1$ μM | $2.1 \pm 0.3$ |
| Curare (ss) | ACH | **9** | **17.4** | 17.5 | | DRC | 100 | $6.3 \pm 0.8$ μM | $2.1 \pm 0.3$ |
| Hexamethonium | ACH | **8.2** | 8.2 | 14.7 | 4 | 1 mM | $61 \pm 2$ | — | — |
| Atropine | ACH | **9.5** | 11.7 | 12.7 | 5 | 1 mM | $47 \pm 6$ | — | — |
| Methylene Blue | — | **4.6** | 7.8 | 14.4 | | DRC | $93 \pm 6$ | $440 \pm 90$ μM | $1.0 \pm 0.2$ |
| Capsaicin | Van | — | — | | 3 | 200 nM | NE | — | — |
| PH 8.5 | Van | — | — | | 3 | — | NE | — | — |
| PH 6.5 | Van | — | — | | 3 | — | NE | — | — |
| Osmolality 400 | Van | — | — | | 3 | — | NE | — | — |
| Osmolality 220 | Van | — | — | | 3 | — | NE | — | — |
| Quinine | Hemi-gap | **9.9** | **13.8** | | | DRC | 100 | $10 \pm 2$ μM | $1.2 \pm 0.11$ |
| Flufenamic Acid | Hemi-gap | 14.9 | 9.4 | 12.05 | 4 | 100 μM | NE | — | — |
| Amiloride* | Na/CNG | **8.3** | 9.9 | 11.3 | | DRC | 100 | $24.2 \pm 0.5$ μM | $2.2 \pm 0.1$ |
| FM1-43** | — | **10.5** | 10.7 | 24.8 | | DRC | 100 | $2.4 \pm 0.3$ μM | $2.2 \pm 0.3$ |

All molecular measurements were from CPK models where cross-sectional areas were determined and the diagonal is given as the diameter of the region. Minimum diameters were determined from the region predicted to enter the channel, typically centred around a charged or partially charged amine (bold values show those with cross-sectional areas smaller than the predicted channel cross-section). The maximum diameter was measured as the largest cross-sectional region, orientated based on the part of the molecule thought to enter the channel (bold indicates those diameters larger than that of the channel). Flufenamic acid values appear reversed due to the requirement of the minimum measurement being about the amine group. The length is the distance between the minimal and maximal diameters. Number of cells indicated by *n* given for drugs where dose–response curve (DRC) not obtained. CNG, cyclic nucleotide-gated; TRP, transient receptor potential; ACh, acetylcholine; Van, vanilloid; hemi-gap, hemi gapjunctional channels; NE, no effect. * Data from Ricci (2002); ** data from Gale *et al.* (2001).

suggest the MET channel is not one of the known vanilloid channels.

### Hemi-gap junctional channels

Several properties of the MET channel, including single channel conductance, calcium block and permeability, as well as non-rectification, are similar to gap junctional and hemi-gap junctional channels (DeVries & Schwartz, 1992). Although these channels are not typically thought of as mechanically gated, the pharmacology was investigated because the biophysical properties of the pore suggested there might be similarities. Quinine, a compound with a variety of actions, both opens and antagonizes hemi-gap junctional channels (Srinivas *et al.* 2001). Quinine also has effects in the auditory system, causing tinnitus and hearing loss (Tange, 1998; Kaltenbach, 2000; Zheng *et al.* 2001). Applied to the apical hair bundle, quinine antagonized the MET current with an $IC_{50}$ of $10 \pm 2$ μM and a Hill coefficient of $1.2 \pm 0.1$ (Fig. 6*A* and *B*). However flufenamic acid, another antagonist of hemi-gap junctional channels (Harks *et al.* 2001; Srinivas & Spray, 2003), had no effect on the MET current (Fig. 6*C*, $n = 4$). So here too results were somewhat ambiguous, suggesting similarities between the hemi-gap pore and the MET pore, but not conclusively identifying the channel type.

### Amine-containing antagonists

At this point the pharmacological data do not clearly classify the channel, as antagonists from each class of compound tested were effective. In an attempt to identify a common mode of action of these compounds, space-filling models were constructed (Fig. 7*A*). Previous findings of

permeable block by FM1-43 (a charged amine derivative; Gale *et al.* 2001) and block by curare (a quarternary amine; Glowatzki *et al.* 1997) indicated that a partially charged amine might be capable of entering the pore electrochemically. The arrows in Fig. 7 point to the partially charged amine for each compound. Note that in each case the amine is in a region of the molecule that is structurally small in size. In addition, it was reasoned that a bulky side chain would be needed to impede flow of the compound through the channel. The side chains are outlined by a rectangle (Fig. 7). Compounds that did not work had sterically hindered amine groups postulated not to be able to enter the channel pore (like nimodipine) or else did not have the partially charged amine group to drive the compound into the channel (Fig. 7*B*). The similarity in structure led to the hypothesis that the compounds were acting as open channel blockers, with the amine penetrating the pore and the side chain preventing permeation. The open channel nature of the block shown in Figs 2 and 3 supports this idea. To test this hypothesis two additional compounds were investigated, curare and methylene blue (Fig. 7*C*). Whereas both compounds have a charged amine to drive the compound into the pore, curare has a side chain to prevent permeation and methylene blue does not, so it is predicted that methylene blue would act as a permeable blocker of the channel.

The first test of this hypothesis was to investigate the actions of tubocurarine, a compound containing a tertiary amine with a large side chain. Curare blocked the MET current (Fig. 8*A* and *B*) with an $IC_{50}$ for the peak response of $16 \pm 1\ \mu M$ and a Hill coefficient of $2.1 \pm 0.3$. As the block became more potent during the stimulation, a dose–response curve was generated from the steady-state response, yielding an $IC_{50}$ of $6.3 \pm 0.8\ \mu M$ and a Hill coefficient of $2.1 \pm 0.3$. As previous data used sinusoidal stimulation to arrive at a steady-state blocking efficacy, comparisons of steady-state values between studies are more appropriate and here the $IC_{50}$ values are in good agreement (Glowatzki *et al.* 1997), suggesting that mammalian and turtle MET channels are pharmacologically similar. The reason for the difference in Hill coefficients (a coefficient of 1 was obtained in the Glowatzki *et al.* 1997 work) is unclear and requires further investigation.

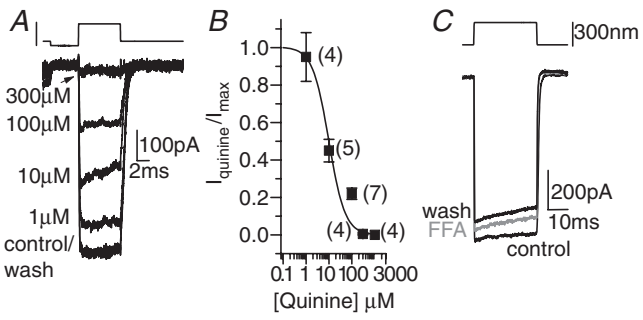


**Figure 6. The hemi-gap junctional channel blockers quinine and flufenamic acid had mixed effects on the MET current**
*A*, responses to maximal stimulation in the presence of varying doses of quinine reveal the dose–response relationship. *B*, normalized current plotted against quinine concentration (■) and fitted with the Hill equation (curve) gave an $IC_{50}$ of $10 \pm 2\ \mu M$ and a Hill coefficient of $1.2 \pm 0.1$ ($r^2 = 0.99$). Flufenamic acid at 200 $\mu M$ had no effect on the MET currents (*C*).

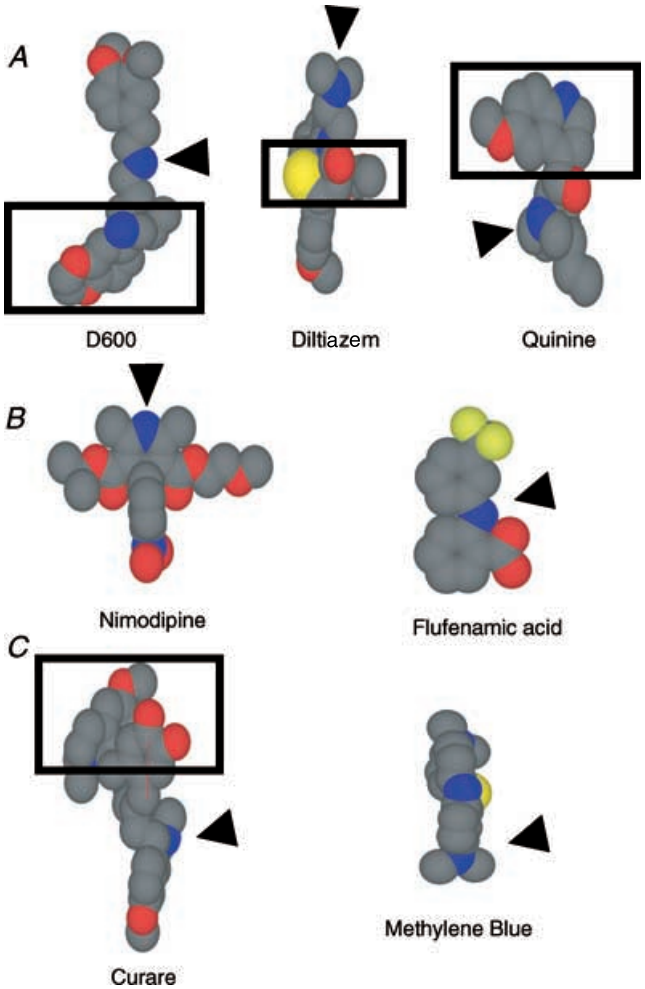


**Figure 7. Space filling models of three tested antagonists (*A*), two ineffective compounds (*B*) and two proposed channel blockers (*C*)**
Grey represents carbon, blue, nitrogen, red oxygen and yellow sulphur. Arrowheads indicate amine proposed to enter the channel pore. Rectangles encompass the side chain proposed to prevent permeation of the compound through the channel. Methylene blue is proposed as a permeable blocker because it does not have a bulky side chain.

The open channel block observed with curare (Fig. 8*A*) was further analysed by plotting the rate of decay of the current at different doses ($1/\tau$) *versus* dose. The linear plot is indicative of a first order reaction and supportive of the open channel nature of the block (Fig. 8*C*) (Armstrong, 1971). The cork-in-bottle model proposed here is first order in that one drug molecule is postulated to interact with one channel to give a blocked channel.

A further test of the open channel nature of the block was the voltage dependence of the block (Fig. 8*D*–*F*) where only inward current was antagonized. This result supports the hypothesis that curare acts as an open channel blocker, driven into and out of the pore electrochemically. The lack of release from block at hyperpolarized potentials indicates that curare is not a permeable blocker of the pore (Zarei & Dani, 1994; Gale *et al.* 2001). The control traces (Fig. 8*D*)

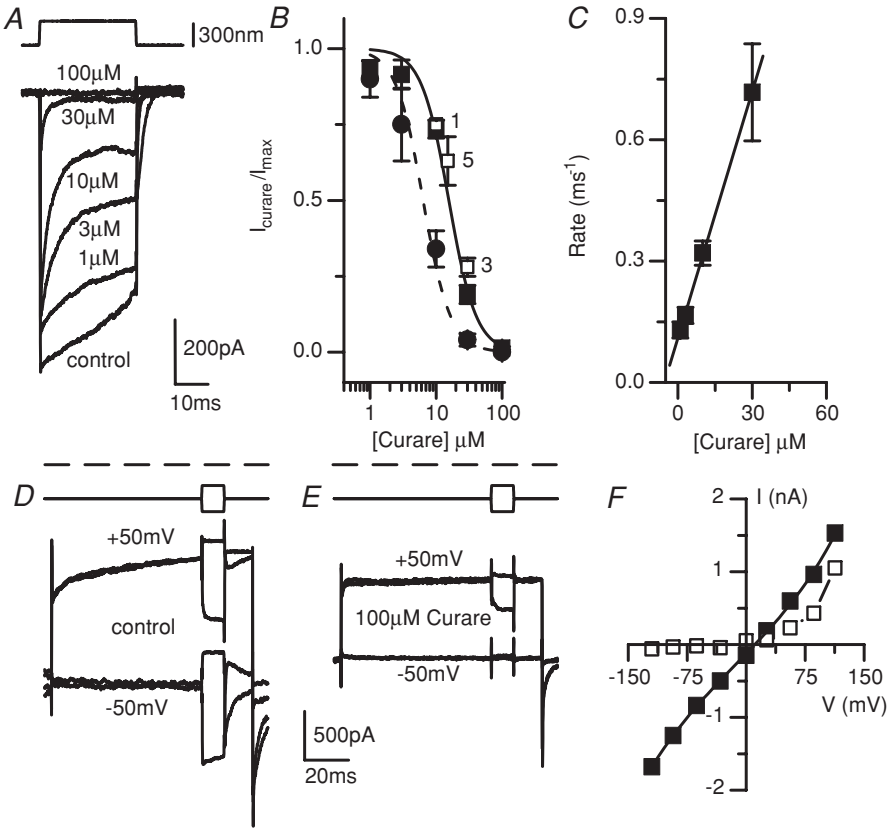


**Figure 8. Tubocurarine is an open channel blocker of the MET current**
*A*, saturating current responses in the absence and presence of various concentrations of curare. A large decrease in current during the stimulation was observed so dose–response curves were plotted for both the peak (■) and steady-state (●) current responses (*B*) ($n = 10$ except for highest dose where $n = 5$). Low frequency cells (□) had sensitivities similar to that of high frequency cells. Low frequency position was $d = 0.34 \pm 0.04$ ($n = 6$). Dose–response curves were fitted to the peak (continuous curve) and steady-state (dashed curve) resulting in $IC_{50}$ values of $16 \pm 1\ \mu$M and $6.3 \pm 0.8\ \mu$M and Hill coefficients of $2.1 \pm 0.3$ for both peak and steady state currents, respectively ($r^2 = 0.99$). *C*, the rate constant was estimated from the fit to the current decay (seen in *A*) at each dose and plotted against concentration. A linear fit with an intercept of $0.11 \pm 0.004\ ms^{-1}$ and a slope of $0.02 \pm 0.002\ ms^{-1}\ \mu M^{-1}$ was applied to the data, indicative of a first order reaction ($r^2 = 0.99$). *D*–*F*, the open channel nature of the block was also confirmed by the reduced block at depolarized potentials. *D* and *E*, examples of the maximal transducer currents obtained at hyperpolarized and depolarized membrane potential in the absence (*D*) and presence (*E*) of 100 $\mu$M curare; mechanical stimulus shown above current traces. Depolarization indicated by dashed line. *F*, a plot of transducer current amplitude against membrane potential in the absence (■) and presence (□) of curare, demonstrating the loss of block at depolarized potentials. The continuous line for control data are fits to the single site barrier model where control values were $k = 0.59 \pm 0.07$, $\delta = 0.45 \pm 0.01$, $V_r = 7 \pm 1$ mV and $V_s = 52 \pm 5$ mV. The curare data was not fitted.

illustrate the non-specific, minimally rectified nature of the channel while in the presence of curare the response becomes rectified. Inward current was completely blocked by curare while outward current at positive potentials was only slightly impeded.

The effect of curare on MET currents from low frequency ($d = 0.3$) cells was also investigated to test whether MET channels varied pharmacologically across frequency positions. Previous work found differences in sensitivity to streptomycin but not to amiloride (Ricci, 2002). No difference in curare efficacy was observed for low frequency cells (Fig. 8*B*). The quarternary ammonium compounds atropine and hexamethonium were also used to further validate the open channel block hypothesis. Both blocked the MET current with an $IC_{50}$ of around 1 mM (see Table 1).

Another test of the open channel hypothesis was performed using methylene blue (Fig. 9), a tertiary amine and known guanylyl cyclase antagonist with no known ion channel effects. Methylene blue was chosen because it has two tertiary amines predicted to penetrate the pore but no large R-group (see Fig. 7, rectangles) to prevent permeation; therefore it is predicted to be a permeant blocker much like FM1-43. Methylene blue antagonized the MET current almost completely at 1 mM, showing a hint of an open channel block (Fig. 9*A* and *B*). Simultaneously with current block the cell turned blue, suggesting that methylene blue was a permeant blocker of the channel. As methylene blue eventually stains all cells, its ability to access the cell cytosol is not limited to passage through the MET channel. However, when MET channels were active the cells stained in 1–3 min whereas when MET channels were not open (due to mechanical disruption during dissection) at least 10 min was required.

Dye passage through the MET channels was confirmed by holding a hair bundle with a stiff probe in a position to close MET channels, preventing staining of the cell while allowing surrounding cells to take up the dye. This experiment was difficult to quantify because adaptation would open some channels despite the probe position and the state of transduction varied between cells so that choosing one cell from a field to study was difficult. So to confirm the initial finding, curare was used to antagonize the action of methylene blue by plugging the pore of the channel. When curare was applied just prior to and simultaneously with methylene blue, cells were prevented from turning blue (Fig. 9*C–E*) in this short time frame. Washing out curare and then applying methylene blue alone resulted in hair cell bodies staining ($n = 3$). Thus, these data support the conclusion that methylene blue is

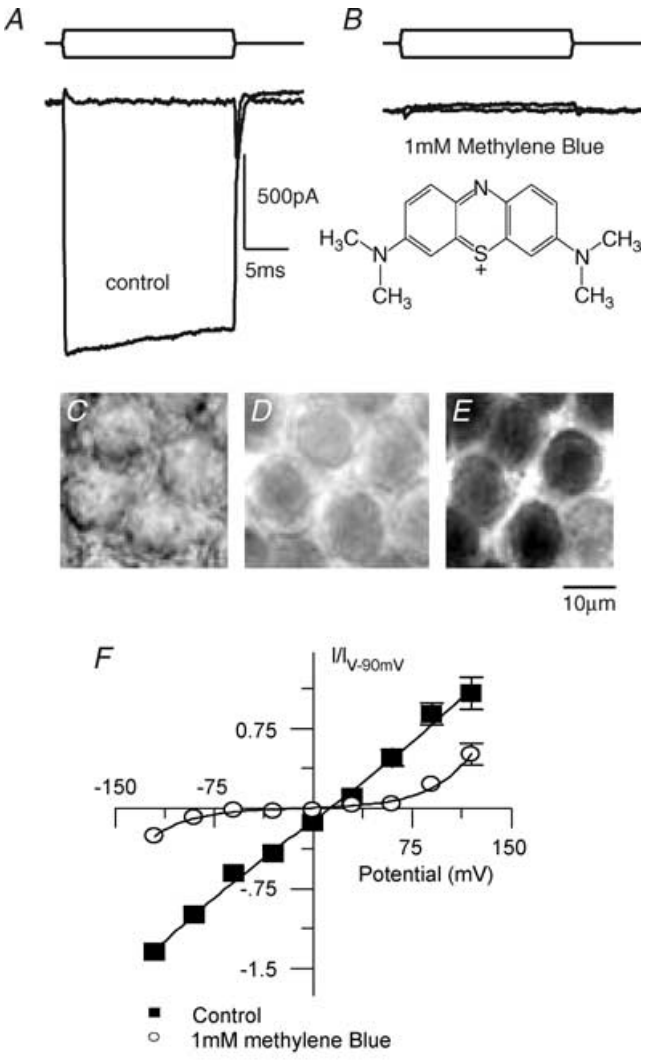


**Figure 9. Methylene Blue (MB) is a permeable blocker of the MET current**

Saturating displacements of the hair bundle in the absence (*A*) and presence (*B*) of 1 mM MB demonstrate current reduction of greater than 90% (stimulus shown above). A slight decrease in current during the stimulus, indicative of an open channel block, was seen in the current trace. *C–E*, MB permeation was antagonized with 100 $\mu$M curare. *C*, Nomarski image of the cell bodies being investigated, prior to drug addition. 5 min incubation in MB (1 mM) and curare (100 $\mu$M) reveals minimal staining (*D*) as compared to the same cells after staining for 5 min with 1 mM MB alone (*E*); scale bar for *C–E* is 10 $\mu$m. An additional test of MB as a permeant blocker of the MET channel was to determine the voltage dependence of block (*F*). Here a similar protocol to that used in Figs 1, 3 and 8 was used in the absence (■) and presence (○) of MB. MB block was reduced at both extremes of polarization. Fits (continuous curve) to the single site binding model (eqn (5)) were $k = 0.8 \pm 0.6$ and $0.007 \pm 0.003$, $\delta = 0.48 \pm 0.04$ and $0.51 \pm 0.06$, $V_r = 8 \pm 4$ mV and $-17 \pm 13$ mV, and $V_s = 85 \pm 54$ mV and $15 \pm 2$ mV for control and in the presence of MB ($n = 3$; $r^2 = 0.99$) for both data sets. S.E.M. bars are shown only when larger than symbol size.

a permeant blocker of the MET channel and support the hypothesis that large charged compounds can enter the channel, both blocking and penetrating the MET channel.

A third test of methylene blue acting as a permeant blocker was the voltage dependence of the block. As mentioned earlier, relief of block at both extremes of potential is indicative of a permeant channel blocker. Protocols like those used in Figs 1, 3 and 8 were used again to examine the voltage dependence of block of methylene blue. In contrast to the effects with curare, methylene blue block was relieved at both positive and negative potentials, supporting the conclusion that methylene blue was a permeant blocker. As the cells turned blue during these experiments it is possible to conclude that the current was carried by methylene blue, in contrast to the previous experiments with diltiazem and D600. The reversal potential shifted −25 mV in the presence of methylene blue, suggesting divalent permeation was blocked before monovalent. The relative distance through the electric field was not different from control ($0.51 \pm 0.06$ and $0.48 \pm 0.04$ for control and in the presence of methylene blue, respectively, $n = 3$). These results are similar to those observed with FM1-43, another permeant blocker of the MET channel (Gale *et al.* 2001).

### Pore width

Together the data suggest that large amines can act as open channel blockers of the MET channels and that drug sensitivities may be in part a function of the presence of an amine group serving to drive the compound into the pore, while a large R-group prevents further permeation. The ability of the charged amine to reach the narrow portion of the channel and the relative size of the channel pore compared to the size of the amine group are predicted to determine drug efficacy. To better quantify the relationship between the molecular dimensions of the drugs and that of the channel pore, experiments were performed to more directly assess channel pore dimensions. The ability of simple amine compounds to permeate channels allows for estimates of channel diameter (Hille, 1971). Simple amines such as methylammonium, trimethylammonium, triethylammonium, tetramethylammonium, tetraethylammonium, tetrapropylammonium and tetrabutylammonium were substituted for sodium and current ratios obtained in order to estimate the size of the MET channel pore. Examples of the currents obtained are displayed in Fig. 10*A*. Relatively large amines showed partial permeability except for the tetrabutyl ammonium. A plot of molecular weight against current ratio (Fig. 10*B*) yields an exponential relationship, demonstrating that the size of the molecule and not binding within the pore dictates current flow and that from the point of view of amine permeability, the pore can be regarded as a molecular sieve (Dwyer *et al.* 1980; McCleskey & Almers, 1985; Sun *et al.* 1997). CPK models of the amines allowed for the minimum cross-section of the molecule to be determined and its diagonal used as an estimate of the molecular diameter. Plotting the radius of the molecule against current ratio allowed for an estimate of pore diameter. The continuous line fitted to these data (eqn (3)) points to the current ratio being a function of the volume of the amine relative to the radius of the pore. This fit corresponds to a pore diameter of $11.6 \pm 0.6$ Å. The parabolic nature of the fit has the slope of the curve becoming positive for larger amines, a result not observed in the data. A slightly better fit was obtained by including a viscous drag component (eqn (4)) proportional to the size of the amine compound (dashed lines). From this model a pore diameter of $12.5 \pm 0.8$ Å was obtained. The viscous drag component flattens the parabolic fit, better representing the data. A problem with this analysis is that $Ca^{2+}$ was required in the external solution during measurements in order to maintain the integrity of the transduction process. As $Ca^{2+}$ most likely binds in the channel pore and affects permeation, these estimates may have some inherent error. If $Ca^{2+}$ permeation was a constant percentage of current flow, regardless of the monovalent ion, then the error will be negligible (based on eqn (4)). If the monovalent permeation is a non-linear function of calcium then we cannot assess the degree of error. However, lowering external $Ca^{2+}$ to 50 $\mu$M did not alter the apparent permeability of the amine (see below), supporting the conclusion that the methodology was reasonable.

### Penetration into the membrane electric field

To further explore the pore region, current–voltage plots were obtained while mechanically stimulating the bundle to maximal 'current on' and 'current off' positions (Fig. 10*D*–*E*) in the presence of different tetra-*n*-alkyl amines. The current traces of Fig. 10*D* demonstrate that the inward currents (at negative potentials) were reduced much more than the outward currents (positive potentials). Plots of the total MET current normalized to the control current in $Na^+$ at −120 mV were plotted for each of the tetra-*n*-alkyl amines in Fig. 10*E* to further illustrate the rectification. These plots were fitted by eqn (5) in order to estimate the relative distance through the membrane electric field

travelled by the cation before blocking or binding. The distance travelled into the membrane electric field in the presence of $Na^+$ was $0.48 \pm 0.03$ ($n = 6$) (presumably $Ca^{2+}$ is the blocking compound). Similar distances were obtained for the amine compounds: $0.41 \pm 0.02$ ($n = 6$) for tetramethylammonium, $0.39 \pm 0.08$ ($n = 6$) for tetraethylammonium and $0.32 \pm 0.07$ for tetrapropylammonium ($n = 6$), suggesting the molecules approached a similar region of the pore. A funnel-shaped pore region is indicated by the slight trend for smaller molecules to penetrate further than larger amines. That each compound could reach a similar position indicates that the mouth of the channel must open rapidly to a vestibule that can accommodate compounds of these

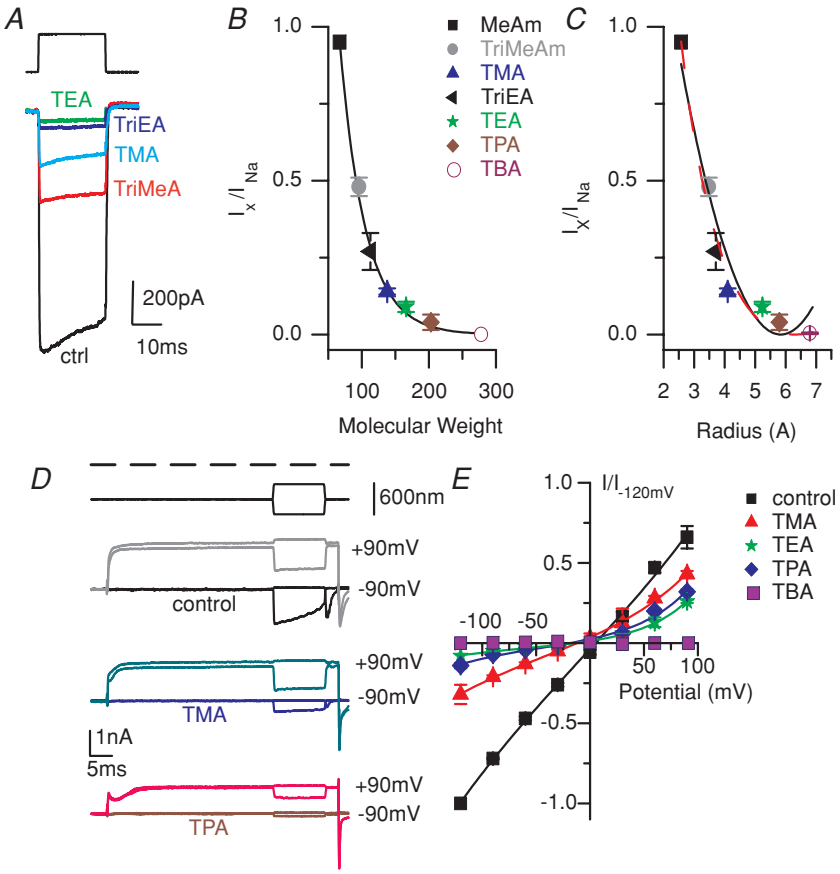


**Figure 10. Permeability to amines allows for an estimate of channel pore diameter**
*A–C*, methylammonium (MeAm), trimethylammonium (TriMeAm), tetramethylammonium (TMA), triethylammonium (TriEA), tetraethylammonium (TEA), tetrapropylammonium (TPA) or tetrabutylammonium (TBA) were substituted for $Na^+$ in the extracellular solution. *A*, examples of peak responses obtained in the different amine solutions. *B*, a plot of $I_{amine}/I_{Na}$ against molecular weight shows an exponential relationship demonstrating that molecular size is the major determinant of current flow. *C*, a plot of $I_{amine}/I_{Na}$ against molecular radii determined from Corey-Pauling-Kolton models allows for the estimate of pore diameter. The continuous curve is the fit to eqn (3) and estimates the pore diameter as $11.6 \pm 0.6$Å ($r^2 = 0.94$), while the dashed curve includes a factor for viscosity (eqn (4)) and estimates a pore diameter of $12.6 \pm 0.8$Å ($r^2 = 0.98$). *D*, the voltage dependence of rectification allowed for the estimate of relative distance through the electric field that the amine permeates. Examples of maximal transducer responses elicited during the stimulus shown at top at a holding potential of $\pm$ 90 mV; voltage stimulus duration shown as dashed line, with $Na^+$ (control), TMA or TPA as the major external monovalent ions. *E*, a plot of current, normalized to the current obtained at 120 mV with extracellular $Na^+$, against membrane potential where black is external $Na^+$ (control), blue is TMA, green is TEA, red is TPA and purple is TBA. The continuous curves represent fits to the single site model of eqn (5). There were 3–6 cells for each compound. The fitted values were as follows: $K = 0.6 \pm 0.3$, $0.12 \pm 0.03$, $0.027 \pm 0.02$ and $0.021 \pm 0.01$, $\delta = 0.48 \pm 0.03$, $0.41 \pm 0.02$, $0.39 \pm 0.08$ and $0.32 \pm 0.07$, $V_r = 9 \pm 4$, $-12 \pm 2$, $-19 \pm 9$ and $-15 \pm 7$ mV and $V_s = 75 \pm 34$, $45 \pm 7$, $29 \pm 8$ and $30 \pm 7$ mV for control, tetramethylammonium, tetraethylammonium, and tetrapropylammonium, respectively ($r^2 > 0.98$ for each).

larger sizes, 14 Å. The reversal potential obtained from these measurements also shifted to hyperpolarized values: $9 \pm 4$ mV for control ($n = 6$), $-12 \pm 2$ mV for tetramethylammonium ($n = 6$), $-19 \pm 9$ mV for tetraethylammonium ($n = 6$) and $-15 \pm 7$ mV for tetrapropylammonium ($n = 6$). Tetrabutylammonium antagonized the current completely at all potentials. Careful examination of the plots of Fig. 10*E* illustrates the difficulty in using reversal potential measurements with this channel. The plot flattens with the amine compounds in a manner similar to that observed with methylene blue, making the estimate of reversal potential difficult; this is also illustrated by the large errors associated with the measurement. An unexpected finding was the reduction of outward current at positive potentials, a phenomenon also observed in other non-specific cation channels where it was argued that the increased hydrophobicity of the larger amines favoured hydrophobic interactions within the channel (French & Shoukimas, 1985; Sanchez *et al.* 1986). Thus entering the channel is more energetically favourable than exiting because the hydrophobic vestibule stabilizes the amine. This type of interaction within the pore might also explain the tetrabutylammonium results, implicating a hydrophobic vestibule in the pore region.

## Pore length

Assuming a cylindrical pore, an estimate of channel diameter and single channel conductance allows an estimate of channel length to be made (eqn (6)). Recent single channel conductance estimates for this papilla location were ~150 pS in 2.8 mM $Ca^{2+}$, while lowering external $Ca^{2+}$ to 50 $\mu$M resulted in a much larger single channel conductance of ~300 pS (Ricci *et al.* 2003). The mechanism responsible for this variation in conductance is unknown. Because experiments were done at 2.8 mM $Ca^{2+}$, the initial estimate of pore length used 150 pS as the single channel conductance in eqn (6), yielding a length of 72 Å, about three times the width of the plasma membrane. Using 300 pS, however, gave an estimate of 31 Å, similar to that for other channels including mechanically gated channels (Cruickshank *et al.* 1997). Assuming a channel length of 72 Å is incorrect suggests that differences in measured values of single channel conductance were not due to a change in the diameter of the pore. That is, perhaps the single channel conductance is a constant but the apparent lower value in high $Ca^{2+}$ was due to rapid flickering behaviour that the recording speed could not resolve. Caution must be exercised with this interpretation because although the channel appears non-rectified in 2.8 mM $Ca^{2+}$ it is clearly rectified in lower $Ca^{2+}$ concentrations (Crawford *et al.* 1991; Ricci *et al.* 2003). This observation suggests that the pore structure is more complex than a simple cylinder. To further test whether pore diameter changed with external $Ca^{2+}$ the relative permeability of tetramethylammonium was measured in normal 2.8 mM and low 50 $\mu$M $Ca^{2+}$, the prediction being that the relative current would increase as extracellular $Ca^{2+}$ was lowered due to a change in pore width from 9 Å (estimated from rearranging eqn (6) to solve for diameter) to 12.5 Å. No difference in relative current flow was observed, however. Lowering extracellular $Ca^{2+}$ relieved the $Ca^{2+}$ block of the channel so the total current amplitude increased (Ricci & Fettiplace, 1998). The ratio of current in 0.05 mM to that in 2.8 mM $Ca^{2+}$ with either $Na^+$ or tetramethylammonium as the monovalent ion did not differ ($1.4 \pm 0.3$ *versus* $1.5 \pm 0.4$: $P > 0.05$, $n = 6$), indicating that the permeability of the amine was unaffected by external $Ca^{2+}$.

Single channel measurements show an increase in conductance with papilla location, suggesting a difference in pore diameter (Ricci *et al.* 2003). A test for a difference in diameter comparing current ratios obtained with tetramethylammonium at high ($0.18 \pm 0.01$, $n = 7$) and low ($0.20 \pm 0.02$, $n = 6$) frequency positions did not reveal any statistical difference ($P > 0.05$). What then might be regulating the single channel conductance? It is possible that the methodology is not sensitive enough to resolve a difference. More experiments are required to better resolve this issue.

Regardless of absolute value, the data suggest the MET channel has a long pore region, consistent with previous measurements indicating the channel may show anomalous mole fraction behaviour (Lumpkin *et al.* 1997).

## Open channel block

The pharmacological data can now be re-evaluated in terms of molecular dimensions as opposed to channel classification. The hypothesis tested earlier was that amine-containing compounds like diltiazem, D600 and tetracaine, acted as open channel blockers where the partially charged amines penetrated the channel pore and the large R-groups attached to the amines prevented further penetration into the channel, like a cork in a bottle. Data obtained with curare, methylene blue, atropine and hexamethonium all support this hypothesis. Cross-sectional areas of each compound were determined from CPK models (Fig. 11*A*). Minimal diameters were

measured about the region of the drug thought to penetrate the channel. As with the amine experiments, the diameter of a circle that the portion of the compound thought to penetrate the channel could pass through was taken as the minimal diameter of the amine. All of the antagonists had a minimal diameter smaller than that of the channel pore, suggesting the compounds could enter the channel and approach its narrowest region (see Table 1 and Fig. 11*B*). A plot of the minimal diameter against $IC_{50}$ shows a good correlation ($r^2 = 0.91$) (Fig. 11*B*). This relationship suggests that the size of molecule binding in the pore dictates occlusion of the pore. Note that atropine, which has its amine in a ring structure, was an outlier in this plot. Perhaps the rigidity of the ring structure sterically limited atropine's ability to penetrate the pore.

The maximal cross-sectional diameter was derived from the region of the drug serving to prevent further penetration of the compound into the channel. Each antagonist, other than methylene blue, had a region whose diameter was greater than that of the estimated minimal pore region (Table 1). Thus both requirements of the cork-in-bottle open channel block hypothesis, first to have a region of the molecule that could penetrate the pore of the channel and second to have a region large enough to prevent permeation through the channel, were met. Methylene blue, having a cross-sectional area smaller than the minimal pore region acted as a permeant blocker of the channel. Those drugs that did not antagonize the channel either did not have minimal areas small enough to enter the channel (flufenamic acid, nimodipine) or else did not have a charged amine to drive the compound into the channel (LY83583 or capsaicin).

Further support for the open channel block theory comes from the correlation between the $IC_{50}$ of the block and the length of the blocking agent (Fig. 11*C*). This relationship suggests the longer the compound, the more potent the block. Here, the idea is that the distance between the charged amine and the bulky R-group determines how close the charged amine can get to the minimal diameter of the pore. However, this correlation only held for the charged amine derivatives and not for other compounds (indicated by open symbols). In fact, the estimated channel length (31 Å) and the estimated distance through the electric field (0.45) give an approximate distance 14 Å into the pore that the drugs need to travel in order to reach the binding site of. Despite these being only crude estimates, the most effective amine compounds had lengths longer than this value, suggesting the amine could reach the binding site while the bulkier portion of the compound could remain near the external face of the channel.

## Discussion

A summary of the compounds tested is given in Table 1. Ten compounds have been identified that antagonize the

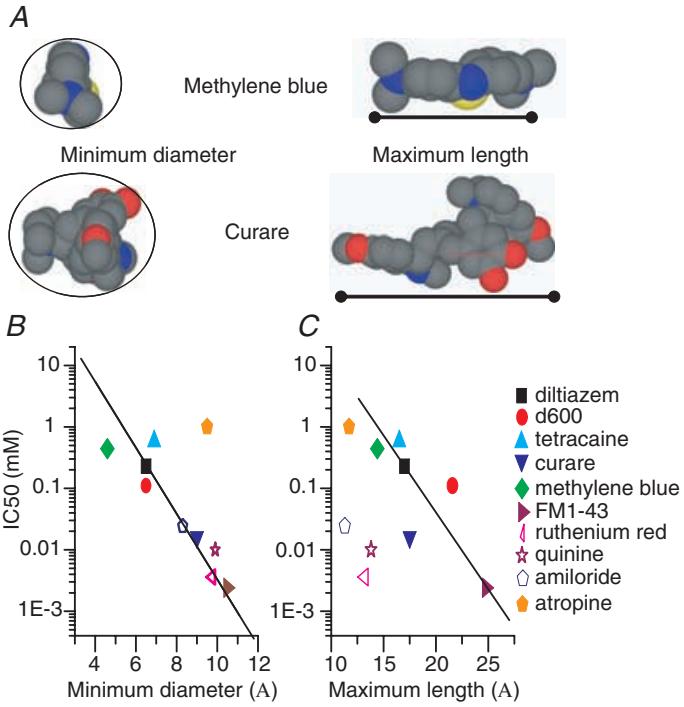


**Figure 11. Molecular dimensions determine drug efficiency**
*A*, space filling models of methylene blue and curare shown to illustrate the measurements used for the analysis. Blue indicates nitrogen, grey indicates carbon, red indicates oxygen and yellow indicates sulphur. The circle around the molecules has a diameter equivalent to the molecule's minimum diameter. The continuous line on the right indicates the measurement for maximum length. *B* plots the $IC_{50}$ of antagonists against minimum width. The filled symbols represent those compounds with clear tertiary or quarternary ammonium compounds while the open symbols represent more complex structures. Both types of compounds were well described in this plot with an $r^2$ value of 0.91. *C*, plots the $IC_{50}$ of each compound against the length, measured from the penetrating amine to the R-group. Compounds that did not have the structure containing the cork-in-bottle topology did not fit the trend. The $r^2$ value was 0.71 for the fit. Log–linear plots were used to better display the range of data.

MET channel: diltiazem, D600, tetracaine, lanthanum, ruthenium red, quinine, curare, atropine, hexamethonium and methylene blue. Five compounds were ineffective as antagonists and neither pH nor osmolality had significant effects on the MET current. This pharmacological profile indicates that the MET channel is unique relative to other non-specific cation channels in that antagonists of CNG, TRP and hemi-gap channels, as well as nicotinic channel blockers, were effective antagonists at hyperpolarized potentials. Although the profile does suggest that the MET channel is most similar to CNG and TRP channels, a caveat to this conclusion is that many of the newly identified TRP and CNG channels have not had complete pharmacological evaluations. A hypothesis is presented regarding drug actions that incorporates the molecular dimensions of the pore. The model also postulates a mechanism for $Ca^{2+}$ permeation and block of the channel. The quantitative estimates of channel dimensions serve to underscore the proposed mechanism of drug action and so are discussed first.

### Molecular dimensions

*n*-Alkyl amines were used to estimate both the minimal pore diameter and its position in the membrane electric field. A diameter of $12.5 \pm 0.8$Å is considerably larger than that reported for other cation channels including nicotinic channels (9.2 Å; Dwyer *et al.* 1980; Dani, 1989), calcium channels (6 Å; McCleskey & Almers, 1985), NMDA channels (7.2 Å; Zarei & Dani, 1995), voltage-gated potassium channels (4.7Å; Bezanilla & Armstrong, 1972), voltage-gated sodium channels (6.1 Å; Hille, 1971)

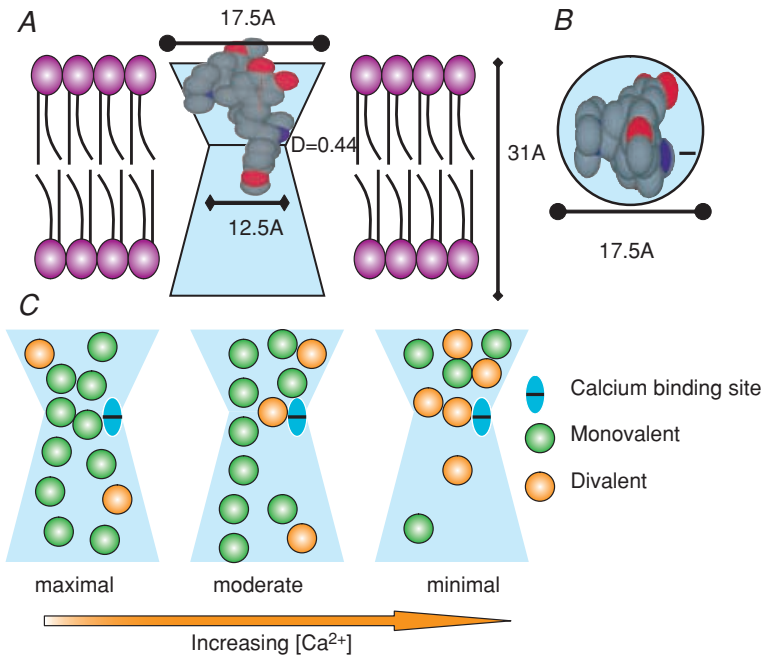


**Figure 12. Schematic representation of a possible blocking scenario supported by the various measurements reported**

*A*, channel depicted as light blue spanning the membrane. The inner portion of the channel is shown for aesthetics, though no measurements are reported regarding its dimensions. Depicted are the width of the smallest portion, the length of the channel and the location of a putative $Ca^{2+}$ binding site. Curare is positioned in the channel to illustrate the block; red indicates oxygen and blue nitrogen. The purple represents lipid. *B* is a top-down view of the channel with curare present, illustrating that room exists for other ions to enter the pore even with curare present. *C* illustrates the proposed ion interaction within the pore that may lead to anomalous mole fraction behaviour and possibly to Hill coefficients greater than 1 for the antagonists. Three scenarios are shown that differ simply in the external concentration of $Ca^{2+}$ present. When $Ca^{2+}$ is low monovalent ions can flow freely with limited interactions with the binding site, indicated as two columns of ion flow (maximal). With higher $Ca^{2+}$, flow is restricted more by $Ca^{2+}$ interacting with the binding site and essentially narrowing the pore, indicated as a single column of ion flow (moderate). When $Ca^{2+}$ is further elevated, the probability of having two $Ca^{2+}$ molecules present increases, so that two ions serve to occlude the channel, despite there only being one binding site (minimal). A similar scenario is proposed for the antagonists, where the antagonist can replace one of the $Ca^{2+}$ molecules.

and CNG channels (9.2 Å; Balabramamian *et al.* 1995). Moreover, the diameter of the MET channel is considerably smaller than that reported for other mechanically gated channels (40Å) (Cruickshank *et al.* 1997). Although making predictions regarding molecular dimensions from macroscopic recordings is not the most precise method, work on gramicidin channels and alamethacin channels has given estimates remarkably close to crystallized structures (Eisenberg *et al.* 1977; Rosenberg & Finkelstein, 1978). The model assumes a symmetrical cylindrical pore that is most likely an oversimplification but allows for comparisons between known channels. The model does not take into account charges within the pore that might serve as a binding site for the amines, though the relationship between the current ratio and molecular weight suggests binding is not an issue (see Sun *et al.* 1997). That the channel acts as a molecular sieve is also supported by the rather small differences in monovalent ion permeabilities (Fig. 1*D* and *E*), despite following an Eisenmann series XI suggestive of a highly electronegative pore (Adams *et al.* 1980).

Another possible source of error is the requirement for extracellular [$Ca^{2+}$] to maintain functional channels, resulting in the use of current ratios as opposed to reversal potential changes to estimate permeability. As $Ca^{2+}$ has a relatively high permeability through the channel, part of the current measured in the presence of amines is likely to be carried by $Ca^{2+}$ (Lumpkin *et al.* 1997; Ricci & Fettiplace, 1998). Several pieces of information support the methodology used. First, that the amines are blocking $Ca^{2+}$ entry and are not simply impermeant ions was demonstrated by current amplitudes approaching zero (Fig. 10*A–C*); previous work demonstrated that impermeant ions leave about 50% of the current to be carried by $Ca^{2+}$ (Ricci & Fettiplace, 1998). Second, the relationship between molecular weight and current ratio suggests that size and not binding dictated the response. Third, when extracellular $Ca^{2+}$ was lowered the current ratios remained constant, suggesting that the current ratio in the presence of amines was a reasonable estimate of permeability. Fourth, the monovalent permeability sequence illustrated in Fig. 1*E*, obtained using current ratios, is in good agreement with previous work in which reversal potentials were used for permeability estimates (Ohmori, 1985). And fifth, the error associated with current ratios would be likely to lead to an overestimate the pore size, reflecting $Ca^{2+}$ permeation rather than amine permeation. However, the permeant block by methylene blue suggests a lower limit to the size of the channel of 7.8 Å and the open channel block by FM1-43 sets a lower limit on channel diameter of 10.5 Å. These values are similar to that estimated using the amines. Together these data are in good agreement and support the validity of the molecular estimates presented.

The distance into the electric field was also estimated using a single site binding model (eqn (5)) to fit MET current voltage plots under a variety of conditions. Regardless of the extracellular ions or blocking agents the relative distance into the electric field was estimated as ∼0.45, a value similar to that obtained in chick (Kimitsuki & Ohmori, 1993), bullfrog (Kroese *et al.* 1989) and mouse (Kros *et al.* 1992; Gale *et al.* 2001), supporting the conclusion that the MET channel is conserved amongst species. This value also suggests that the blocking site for $Ca^{2+}$ must be different from the binding site for fast adaptation site, simply based on location (Crawford *et al.* 1991; Ricci & Fettiplace, 1998). A single site binding model is most probably an oversimplification but has proven adequate for representing the data presented here.

Recent data have shown a tonotopic variation in the single channel conductance, with conductance ranging from 150 to 300 pS in 50 $\mu$M external calcium (Ricci *et al.* 2003) at −80 mV. This variation would predict a change in pore diameter from 9 to 12.5 Å. Attempts at determining different pharmacological sensitivities based on this anticipated difference in channel pore diameter failed, however. Curare, for example, had no significant difference in $IC_{50}$ for block at high or low frequency positions, nor was there a difference in permeability ratio for tetramethylammonium. It is possible that compounds with more subtle structural differences are required to differentiate between the channels at different frequency locations. Another possibility is that much as in CNG channels, $Ca^{2+}$ binding within the pore regulates permeability and it is the efficacy of $Ca^{2+}$ and not the physical diameter that varies (see Fig. 12*C*) (Dzeja *et al.* 1999). It is also possible that the interpretation regarding pore diameter differences is incorrect and that the estimated differences in channel length, not width dictate current flow. If the pore length varies tonotopically and the channel width remains constant then no pharmacological differences would necessarily be predicted for open channel blockers.

Assuming a single channel conductance of 300 pS, the length of the channel was estimated as ∼31 Å, indicating a long pore containing multiple ions simultaneously. The estimate of length is based on the assumption of a cylindrical pore that has a non-rectifying MET current. Evidence from single channel recordings (Ricci *et al.*

2003) and current–voltage plots (Crawford *et al.* 1991) suggests that at low external $Ca^{2+}$ concentrations the channel is partially rectified, however, and thus might invalidate this estimate. The actions of $Ca^{2+}$ within the pore need further investigation to reconcile this issue.

### Open channel block

The pharmacological data revealed that antagonists from a variety of channel classes were effective blockers of the MET channel. To account for the pharmacological profile an open channel hypothesis regarding the mechanism of block is proposed that is consistent with reported data and should serve to be predictive when identifying new antagonists. This hypothesis may also prove to be generally applicable to the larger conductance non-specific cation channels. An effective open channel blocker needs a cross-sectional area measured about the charged amine of less than the channel's minimal width and an R-group with a diameter larger than the pore width in order to prevent permeation. A variety of data support this model. First, all antagonists had a minimum diameter that was less than the channel width (Table 1). Those amine-containing compounds that blocked the channel also had regions whose width was larger than that of the pore (Table 1 and Fig. 11). Compounds that did not meet these criteria did not produce block. Second, the exponential decay in current in response to saturating bundle displacements during the block by curare, D600 and diltiazem also support the open channel block theory. Third, the linear plot of blocking rate against doseage for diltiazem, D600 and curare supports a first order reaction consistent with an open channel block. Fourth, the voltage dependence of the block by curare, D600 and diltiazem reflects an open channel block and that of methylene blue a permeant block. And fifth, the correlation between minimal diameter of the antagonists and $IC_{50}$, as well as the correlation between drug length and $IC_{50}$, support the proposed hypothesis.

One apparent complication with the model is that, while the voltage dependence of block by D600 and diltiazem suggest a permeable block (having block relieved at both positive and negative potentials), the molecular dimensions of these compounds suggest that they cannot penetrate through the channel pore. The explanation for this apparent disparity is that at negative potentials monovalent ions are electrochemically driven past the drugs and that it is not the drugs carrying the current. The larger compound, curare, does not show this relief of block, most probably because it plugs the pore more completely than either of these two compounds. This hypothesis is supported by the second complication of the model, that the Hill coefficients tend to be greater than 1, implying that one molecule of the drug is not sufficient to completely antagonize current flow. It is possible, however, that the pore of the channel is compliant and that large polarizations can force the molecule through the channel despite the difference in estimated molecular dimensions.

Hill coefficients greater than 1 for most compounds tested suggests either cooperativity in the blocking action or the requirement for multiple molecules of drug for block. Since none of the antagonists described has a geometry that would allow multiple molecules into the channel pore (see Fig. 11), this finding might suggest the hypothesis is inaccurate. However, a likely explanation for this phenomenon comes from the finding that ions interact within the pore of the channel and that $Ca^{2+}$ is a channel antagonist (Lumpkin *et al.* 1997; Ricci & Fettiplace, 1998). The hypothesis is that $Ca^{2+}$ and the other antagonists work together to block current flow. The rationale for this hypothesis is depicted schematically in Fig. 12*C* in the absence of antagonists. $Ca^{2+}$ binds at a site within the pore that serves to limit current flow either by electrostatic repulsion or physically narrowing the width of the pore. Figure 12*C* depicts this effect as the pore passing one ion when $Ca^{2+}$ is bound and two ions when $Ca^{2+}$ is not. At low external $Ca^{2+}$ concentrations the likelihood of $Ca^{2+}$ binding at the site is reduced so the block is reduced and current flow is increased. As $Ca^{2+}$ is elevated, the likelihood of its being found at the binding site increases, thus current flow is reduced. Further elevation allows for $Ca^{2+}$ to be at the binding site and also in the pore, a scenario that occludes current flow. This particular representation was chosen for its ease of presentation. It is also possible that binding to a site at this narrow region slows current flow through the channel, so that $Ca^{2+}$ binding results in slower flow than does $Na^{+}$ binding. When an antagonist is introduced extracellularly into the system where $Ca^{2+}$ is already having some blocking action, the antagonist block will sum with the $Ca^{2+}$ block but may also potentiate the block of $Ca^{2+}$ by narrowing the pore diameter. In either case the interaction between these blockers may be responsible for the Hill coefficient being greater than 1. Using Fig. 12*C* to illustrate the point, the antagonists will allow current flow only when monovalent ions are present (maximal) so that both the moderate and minimal states are now blocked when antagonist is present. Macroscopic current measurements would appear to pass monovalents preferentially because the moderate state would no longer be

passing $Ca^{2+}$. As can be seen from the schematic diagram in Fig. 12*B*, although multiple antagonist molecules cannot fit into the channel pore, even with this simple cylindrical type pore, there is space for other molecules like $Ca^{2+}$. It is via these spaces that ions are predicted to be forced through the channel with larger polarizations (i.e. voltage dependence of D600 and diltiazem). This mechanism of block is supported by the relationship between $IC_{50}$ and the diameter of the narrowest region of the antagonists. It is further supported by the decrease in adaptation, indicative of a loss of $Ca^{2+}$ permeation prior to a significant loss of MET current. And finally it is supported by the negative shift in reversal potential in the presence of blockers, suggesting that channels are passing monovalent ions.

### External mouth of the channel

Given the hypothesis of an open channel block, not only does the compound need a region small enough to enter the channel, the mouth of the channel needs to be large enough to accept the blocking portion of the drug. Thus, the mouth of the pore need be at least 17Å wide in order for curare's maximum width (largest compound tested) to fit and for the charged amine to reach the minimum channel width (Fig. 12*A*). This is supported by the data demonstrating that each amine, including curare, penetrated a similar relative distance, ∼45% into the membrane electric field. That this distance remained constant, even for the control condition, implies that these compounds can penetrate a similar distance which requires the mouth of the pore to be wide.

In conclusion, these investigations provide information regarding several aspects of the MET channel pore. First, they provide a pharmacological profile for the MET channel that can be used in its molecular identification and characterization. The pharmacology of the channel suggests the pore is most like that of CNG and TRP type channels. Second, the pharmacological information can be used to identify new antagonists that may have value both experimentally and clinically. Third, the dimensions of the channel pore, including its length, width, the shape of the external mouth and the location of the minimum diameter site relative to the membrane electric field, were estimated. Fourth, a hypothesis regarding open channel block by $Ca^{2+}$ and the antagonists is presented that is consistent with all data presented and those in the literature. The model incorporates an interaction between $Ca^{2+}$ and antagonists to account for Hill coefficients greater than 1. Future work will incorporate both theoretical and further biophysical analysis of the pore to test the proposed mechanism.

## References


Adams DJ, Dwyer TM & Hille B (1980). The permeability of endplate channels to monovalent and divalent metal cations. *J General Physiol* **75**, 493–510.

Armstrong CM (1971). Interaction of tetraethylammonium ion derivatives with the potassium channels of giant axons. *J General Physiol* **58**, 413–437.

Assad JA, Shepherd GM & Corey DP (1991). Tip-link integrity and mechanical transduction in vertebrate hair cells. *Neuron* **7**, 985–994.

Balabramamian S, Lynch JW & Barry PH (1995). The permeation of organic cations through cAMP-gated channels in mammalian olfactory receptor neurons. *J Memb Biol* **146**, 177–191.

Benham CD, Davis JB & Randall AD (2002). Vanilloid and TRP channels: a family of lipid-gated cation channels. *Neuropharmacology* **42**, 873–888.

Bezanilla F & Armstrong CM (1972). Negative conductance caused by entry of sodium and cesium ions into the potassium channels of squid axons. *J General Physiol* **60**, 588–608.

Brown RL, Haley TL, West KA & Crabb JW (1999). Pseudechetoxin: a peptide blocker of cyclic nucleotide-gated ion channels. *Proc Natl Acad Sci U S A* **96**, 754–759.

Clapham DE, Runnels LW & Strubing C (2001). The TRP ion channel family. *Nat Rev Neurosci* **2**, 387–396.

Corey DP (2003). New TRP channels in hearing and mechanosensation. *Neuron* **39**, 585–588.

Corey DP & Hudspeth AJ (1979). Ionic basis of the receptor potential in a vertebrate hair cell. *Nature* **281**, 675–677.

Crawford AC, Evans MG & Fettiplace R (1989). Activation and adaptation of transducer currents in turtle hair cells. *J Physiol* **419**, 405–434.

Crawford AC, Evans MG & Fettiplace R (1991). The actions of calcium on the mechano-electrical transducer current of turtle hair cells. *J Physiol* **434**, 369–398.

Crawford AC & Fettiplace R (1985). The mechanical properties of ciliary bundles of turtle cochlear hair cells. *J Physiol* **364**, 359–379.

Cruickshank CC, Minchin RF, Le Dain AC & Martinac B (1997). Estimation of the pore size of the large-conductance mechanosensitive ion channel of Escherichia coli. *Biophys J* **73**, 1925–1931.

Dani JA (1989). Open channel structure and ion binding sites of the nicotinic acetylcholine receptor channel. *J Neurosci* **9**, 884–892.

DeVries SH & Schwartz EA (1992). Hemi-gap-junction channels in solitary horizontal cells of the catfish retina. *J Physiol* **445**, 201–230.

Drescher MJ, Barretto RL, Chaturvedi D, Beisel KW, Hatfield JS, Khan KM & Drescher DG (2002). Expression of subunits for the cAMP-sensitive 'olfactory' cyclic nucleotide-gated ion channel in the cochlea: implications for signal transduction. *Brain Res Mol Brain Res* **98**, 1–14.

Dwyer TM, Adams DJ & Hille B (1980). The permeability of the endplate channel to organic cations in frog muscle. *J General Physiol* **75**, 469–492.

Dzeja C, Hagen V, Kaupp UB & Frings S (1999). $Ca^{2+}$ permeation in cyclic nucleotide-gated channels. *EMBO J* **18**, 131–144.

Eatock RA, Corey DP & Hudspeth AJ (1987). Adaptation of mechanoelectrical transduction in hair cells of the bullfrog's sacculus. *J Neurosci* **7**, 2821–2836.

Edsall JT & McKenzie HA (1978). Water and proteins. I. The significance and structure of water; its interaction with electrolytes and nonelectrolytes. *Adv Biophys* **10**, 137–207.

Eisenberg M, Kleinberg ME & Shaper JH (1977). Channels across black lipid membranes. *Ann N Y Acad Sci* **303**, 281–294.

Fettiplace R, Ricci AJ & Hackney CM (2001). Clues to the cochlear amplifier from the turtle ear. *Trends Neurosci* **24**, 169–175.

Fodor AA, Black KD & Zagotta WN (1997). Tetracaine reports a conformational change in the pore of cyclic nucleotide-gated channels. *J General Physiol* **110**, 591–600.

French RJ & Shoukimas JJ (1981). Blockage of squid axon potassium conductance by internal tetra-N-alkylammonium ions of various sizes. *Biophys J* **34**, 271–291.

French RJ & Shoukimas JJ (1985). An ion's view of the potassium channel. The structure of the permeation pathway as sensed by a variety of blocking ions. *J General Physiol* **85**, 669–698.

Frings S, Lynch JW & Lindemann B (1992). Properties of cyclic nucleotide-gated channels mediating olfactory transduction. Activation, selectivity, and blockage. *J General Physiol* **100**, 45–67.

Gale JE, Marcotti W, Kennedy HJ, Kros CJ & Richardson GP (2001). FM1-43 dye behaves as a permeant blocker of the hair-cell mechanotransducer channel. *J Neurosci* **21**, 7013–7025.

Geleoc GS, Lennan GW, Richardson GP & Kros CJ (1997). A quantitative comparison of mechanoelectrical transduction in vestibular and auditory hair cells of neonatal mice. *Proc Roy Soc Lond* **264**, 611–621.

Glowatzki E, Ruppersberg JP, Zenner HP & Rusch A (1997). Mechanically and ATP-induced currents of mouse outer hair cells are independent and differentially blocked by d-tubocurarine. *Neuropharmacology* **36**, 1269–1275.

Gunthorpe MJ, Benham CD, Randall A & Davis JB (2002). The diversity in the vanilloid (TRPV) receptor family of ion channels. *Trends Pharmacol Sci* **23**, 183–191.

Halaszovich CR, Zitt C, Jungling E & Luckhoff A (2000). Inhibition of TRP3 channels by lanthanides. Block from the cytosolic side of the plasma membrane. *J Biol Chem* **275**, 37423–37428.

Harks EG, de Roos AD, Peters PH, de Haan LH, Brouwer A, Ypey DL, van Zoelen EJ & Theuvenet AP (2001). Fenamates: a novel class of reversible gap junction blockers. *J Pharmacol Exp Ther* **298**, 1033–1041.

Hille B (1968). Pharmacological modifications of the sodium channels of frog nerve. *J General Physiol* **51**, 199–219.

Hille B (1971). The permeability of the sodium channel to organic cations in myelinated nerve. *J General Physiol* **58**, 599–619.

Hille B (1973). Potassium channels in myelinated nerve. *J General Physiol* **61**, 669–686.

Holton T & Hudspeth AJ (1986). The transduction channel of hair cells from the bull-frog characterized by noise analysis. *J Physiol* **375**, 195–227.

Jorgensen F & Ohmori H (1988). Amiloride blocks the mechano-electrical transduction channel of hair cells of the chick. *J Physiol* **403**, 577–588.

Kaltenbach JA (2000). Neurophysiologic mechanisms of tinnitus. *J Am Acad Audiol* **11**, 125–137.

Kellenberger S & Schild L (2002). Epithelial sodium channel/degenerin family of ion channels: a variety of functions for a shared structure. *Physiol Rev* **82**, 735–767.

Kimitsuki T, Nakagawa T, Hisashi K, Komune S & Komiyama S (1993). Cisplatin blocks mechano-electric transducer current in chick cochlear hair cells. *Hear Res* **71**, 64–68.

Kimitsuki T, Nakagawa T, Hisashi K, Komune S & Komiyama S (1996). Gadolinium blocks mechano-electric transducer current in chick cochlear hair cells. *Hear Res* **101**, 75–80.

Kimitsuki T & Ohmori H (1993). Dihydrostreptomycin modifies adaptation and blocks the mechano-electric transducer in chick cochlear hair cells. *Brain Res* **624**, 143–150.

Kleene SJ (2000). Spontaneous gating of olfactory cyclic-nucleotide-gated channels. *J Membr Biol* **178**, 49–54.

Kolesnikov SS, Rebrik TI, Zhainazarov AB, Tavartkiladze GA & Kalamkarov GR (1991). A cyclic-AMP-gated conductance in cochlear hair cells. *FEBS Lett* **290**, 167–170.

Kraske S, Cunningham JT, Hajduczok G, Chapleau MW, Abboud FM & Wachtel RE (1998). Mechanosensitive ion channels in putative aortic baroreceptor neurons. *Am J Physiol* **275**, H1497–H1501.

Kraus R, Reichl B, Kimball SD, Grabner M, Murphy BJ, Catterall WA & Striessnig J (1996). Identification of benz(othi)azepine-binding regions within L-type calcium channel alpha1 subunits. *J Biol Chem* **271**, 20113–20118.

Kroese AB, Das A & Hudspeth AJ (1989). Blockage of the transduction channels of hair cells in the bullfrog's sacculus by aminoglycoside antibiotics. *Hear Res* **37**, 203–217.

Kros CJ, Rusch A & Richardson GP (1992). Mechano-electrical transducer currents in hair cells of the cultured neonatal mouse cochlea. *Proc R Soc Lond B Biol Sci* **249**, 185–193.

Lane JW, McBride DW Jr & Hamill OP (1993). Ionic effects on amiloride block of the mechanosensitive channel in Xenopus oocytes. *Br J Pharmacol* **108**, 116–119.

Leinders-Zufall T & Zufall F (1995). Block of cyclic nucleotide-gated channels in salamander olfactory receptor neurons by the guanylyl cyclase inhibitor LY83583. *J Neurophysiol* **74**, 2759–2762.

Liedtke W, Choe Y, Marti-Renom MA, Bell AM, Denis CS, Sali A, Hudspeth AJ, Friedman JM & Heller S (2000). Vanilloid receptor-related osmotically activated channel (VR-OAC), a candidate vertebrate osmoreceptor. *Cell* **103**, 525–535.

Lumpkin EA & Hudspeth AJ (1995). Detection of Ca2+ entry through mechanosensitive channels localizes the site of mechanoelectrical transduction in hair cells. *Proc Natl Acad Sci U S A* **92**, 10297–10301.

Lumpkin EA, Marquis RE & Hudspeth AJ (1997). The selectivity of the hair cell's mechanoelectrical-transduction channel promotes Ca2+ flux at low Ca2+ concentrations. *Proc Natl Acad Sci U S A* **94**, 10997–11002.

McCleskey EW & Almers W (1985). The Ca channel in skeletal muscle is a large pore. *Proc Natl Acad Sci U S A* **82**, 7149–7153.

Maingret F, Fosset M, Lesage F, Lazdunski M & Honore E (1999). TRAAK is a mammalian neuronal mechano-gated K+ channel. *J Biol Chem* **274**, 1381–1387.

Montell C, Birnbaumer L & Flockerzi V (2002). The TRP channels, a remarkably functional family. *Cell* **108**, 595–598.

Ohmori H (1985). Mechano-electrical transduction currents in isolated vestibular hair cells of the chick. *J Physiol* **359**, 189–217.

Ohmori H (1987). Gating properties of the mechano-electrical transducer channel in the dissociated vestibular hair cell of the chick. *J Physiol* **387**, 589–609.

Ricci A (2002). Differences in mechano-transducer channel kinetics underlie tonotopic distribution of fast adaptation in auditory hair cells. *J Neurophysiol* **87**, 1738–1748.

Ricci AJ, Crawford AC & Fettiplace R (2000). Active hair bundle motion linked to fast transducer adaptation in auditory hair cells. *J Neurosci* **20**, 7131–7142.

Ricci AJ, Crawford AC & Fettiplace R (2003). Tonotopic variation in the conductance of the hair cell mechanotransducer channel. *Neuron* **40**, 983–990.

Ricci AJ & Fettiplace R (1997). The effects of calcium buffering and cyclic AMP on mechano-electrical transduction in turtle auditory hair cells. *J Physiol* **501**, 111–124.

Ricci AJ & Fettiplace R (1998). Calcium permeation of the turtle hair cell mechanotransducer channel and its relation to the composition of endolymph. *J Physiol* **506**, 159–173.

Ricci AJ, Wu YC & Fettiplace R (1998). The endogenous calcium buffer and the time course of transducer adaptation in auditory hair cells. *J Neurosci* **18**, 8261–8277.

Rosenberg PA & Finkelstein A (1978). Water permeability of gramicidin A-treated lipid bilayer membranes. *J General Physiol* **72**, 341–350.

Rusch A, Kros CJ & Richardson GP (1994). Block by amiloride and its derivatives of mechano-electrical transduction in outer hair cells of mouse cochlear cultures. *J Physiol* **474**, 75–86.

Sanchez JA, Dani JA, Siemen D & Hille B (1986). Slow permeation of organic cations in acetylcholine receptor channels. *J General Physiol* **87**, 985–1001.

Schnee ME & Ricci AJ (2003). Biophysical and pharmacological characterization of voltage-gated calcium currents in turtle auditory hair cells. *J Physiol* **549**, 697–717.

Shotwell SL, Jacobs R & Hudspeth AJ (1981). Directional sensitivity of individual vertebrate hair cells to controlled deflection of their hair bundles. *Ann N Y Acad Sci* **374**, 1–10.

Sidi S, Friedrich RW & Nicolson T (2003). NompC TRP channel required for vertebrate sensory hair cell mechanotransduction. *Science* **301**, 96–99.

Srinivas M, Hopperstad MG & Spray DC (2001). Quinine blocks specific gap junction channel subtypes. *Proc Natl Acad Sci U S A* **98**, 10942–10947.

Srinivas M & Spray DC (2003). Closure of gap junction channels by arylaminobenzoates. *Mol Pharmacol* **63**, 1389–1397.

Strassmaier M & Gillespie PG (2003). Fast adaptation in the mammalian cochlea: a conserved mechanism for cochlear amplification. *Nat Neurosci* **6**, 790–791.

Sun YM, Favre I, Schild L & Moczydlowski E (1997). On the structural basis for size-selective permeation of organic cations through the voltage-gated sodium channel. Effect of alanine mutations at the DEKA locus on selectivity, inhibition by Ca2+ and H+, and molecular sieving. *J General Physiol* **110**, 693–715.

Tange RA (1998). Ototoxicity. *Adverse Drug React Toxicol Rev* **17**, 75–89.

Tucker TR & Fettiplace R (1996). Monitoring calcium in turtle hair cells with a calcium-activated potassium channel. *J Physiol* **494**, 613–626.

Walker RG, Willingham AT & Zuker CS (2000). A Drosophila mechanosensory transduction channel. *Science* **287**, 2229–2234.

Wilkinson NC, Gao F & Hamill OP (1998). Effects of mechano-gated cation channel blockers on Xenopus oocyte growth and development. *J Membr Biol* **165**, 161–174.

Woodhull AM (1973). Ionic blockage of sodium channels in nerve. *J General Physiol* **61**, 687–708.

Zarei MM & Dani JA (1994). Ionic permeability characteristics of the N-methyl-D-aspartate receptor channel. *J General Physiol* **103**, 231–248.

Zarei MM & Dani JA (1995). Structural basis for explaining open-channel blockade of the NMDA receptor. *J Neurosci* **15**, 1446–1454.

Zheng J, Ren T, Parthasarathi A & Nuttall AL (2001). Quinine-induced alterations of electrically evoked otoacoustic emissions and cochlear potentials in guinea pigs. *Hear Res* **154**, 124–134.

Zufall F & Firestein S (1993). Divalent cations block the cclic nucleotide-gated channel of the olfactory receptor neurons. *J Neurophysiol* **69**, 1758–1768.

## Acknowledgements

This work was supported by NIDCD grant RO1 DC03896 to A.J.R. and the American Tinnitus Association. Our thanks to Dr Takashi Morita at Meiji Pharmaceutical University, Japan for his generous donation of the pseudecatoxin. Thanks also to Drs Katherine Rennie, Geoff Schofield, Mike Schnee and Robert Fettiplace for careful reading of this manuscript.